THE UNIVERSITY OF NOTTINGHAM

SCHOOL OF ELECTRICAL AND
ELECTRONIC ENGINEERING

Development of a bidirectional software interface to couple laser diode simulation software (CONAN) to optical modeling software

AUTHOR Mr. R.C.I. MacKenzie

SUPERVISOR Professor E.C. Larkins

DATE May 2004

Abstract:
A bidirectional interface coupling a high powered tapered laser simulator and an optical simulator is developed. The developed system is then used to examine the effects of light reflected off optical components reentering the laser's cavity. The laser/optical system is shown to behave as a composite cavity. Experiments are then performed to minimize these effects by changing the design of the laser. A method for minimizing the effect of back reflections is developed. It is also shown that back reflections can enhance the laser's performance.

Forth year project thesis submitted in part fulfillment of the requirements of the degree of Master of Engineering.

ACKNOWLEDGMENTS

I wish to thank my supervisor Professor E.C. Larkins for his excellent guidance, help , support and patience throughout this project. Dr. Matthew Clark was of great assistance on more than one occasion during the project and introduced me to some very good literature concerning Fourier Optics. I am very grateful to Stephen Bull for his assistance throughout this project. Also I would like to thank Philip Bream for his useful and constructive criticism. With out the help of these people, this thesis would not have been possible.

Content

1. Introduction

A general introduction to the problem

1.1 Introduction

In recent years the use of laser diodes has become widespread. They are commonly used in a variety of applications ranging from telecommunications right through to medicine. They have become more attractive than their gas and solid state counterparts due their robustness, small size, high efficiency, and low cost per unit. For many applications, a coherent beam of high brightness is required. High power laser diodes have been produced, but they suffer from poor beam quality. For example, the laser may lase in more that one mode, so the emitted light may not be coherent or side lobes may be produced. Recent improvements in laser technology have concerned themselves with the internal structure of the laser as a signal isolated device [2], however a laser is seldom used in isolation - it is normally part of an optical system, with its light passed through optical components, e.g. lenses, filters, diffraction gratings or fiber optics, before the light energy is used. It is clear that light could reflect off the optical components and back into the laser cavity (Fig 1.1), effectively creating a composite cavity laser. This supposition is justified when it is considered that a the reflectivity of common glass is 5%, and a typical laser diodes front-facet is covered in an anti reflective coating with a reflectivity ranging from 0.01% to 5%. It has been shown by experiment that the light reentering the laser cavity can have a significant impact on the quality of the beam [7],[8],[9]. The effects can be both positive and negative, either causing interference, constructive or destructive [7], frequency stabilization [9], or even hysteresis [7].

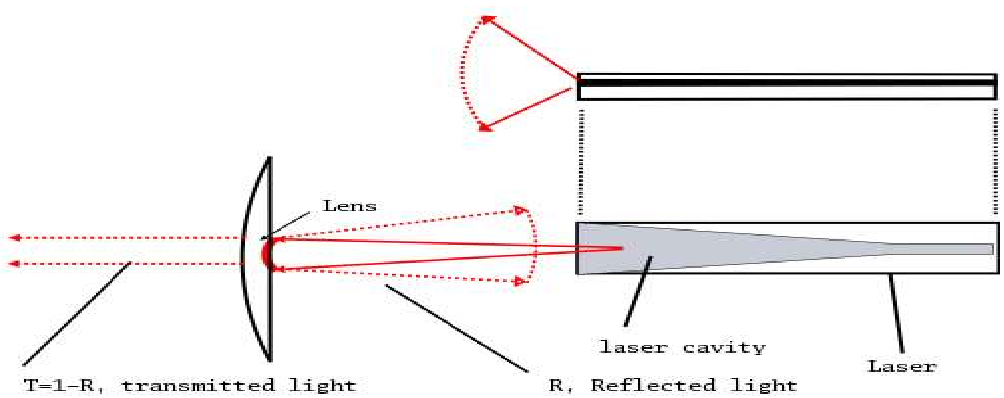

Figure 1.1 Back reflected light from the optical components to the laser.
A typical broad area laser diode is shown.

This project will computationally investigate the effects of optical feedback, by coupling state-of-the-art laser diode modeling software (CONAN) to advanced optical simulation software. By coupling these elements, a model will be produced, which is capable of simulating the linear and nonlinear properties of the laser-optical system. It is hoped that a better understanding of the feedback effects will be gained so that in future systems feedback can be minimized or used to improve beam quality.

1.2 Explanation of industrial relevance

Since the creation of high power laser diodes, laser diode technology has been experiencing a major technological change. What used to be viewed as a device for purely low power communications and sensing applications is now making major inroads in to space telecommunication [23], nonlinear optical frequency conversion [24], medical treatments [25] and material processing [26]. When one considers their small size ($<1\text{cm}^3$)[26], large maintenance interval (> $1\,x10^4 h$)[26], low price (<100$ W^{-1})[26] and an efficiency of well over 50%, they are an attractive alternative to their large, inefficient, expensive, gas and solid state counterparts. However, for high power applications, the optical mode volume of the semiconductor laser source has to be large [21] in order to reduce junction temperature and the optical power density at the facets. Failure to do so may result in reliability problems and the destruction of the device[22]. These requirements lead to the design of broad area devices [23], such as tapered lasers, alpha-distributed-feedback ($\alpha - DFB$) lasers, antiresonant reflection and optical wave guide (ARROW) lasers. Of these new devices, the tapered laser shows the greatest promise due to its simplicity of operation and ease of fabrication. Both these factors make the mass production of device more feasible. Its optical and electron confinement is provided by means of a heterostructure comprised of layers with different reflective indices and band gaps. This electron and optical confinement is advantageous from the point of view of electrical efficiency and temperature control, but due to the very confined vertical lasing mode (4um) produced by the wave-guide, the beam diffracts in the vertical (fast) axis at an angle of over 20 degrees. This requires corrective optics normally in the form of a cylindrical lens placed very close to the front facit (1mm). As soon as one places any reflecting surface in front of a high power laser, composite cavity effects will be experienced and beam quality will be degraded. In the extreme case this beam quality degaradation may even result in filmentation due to the excess power linked back in to the device. All in all, engineers in the field today do not know what will happen to the beam quality of a laser if a lens is placed in front of it. This has the potential to introduce fundamental flaws into a system which could result to unnecessary costs being incurred later on the system life cycle due to redesigns or component failures. By clarifying the issues associated with feedback, an engineer will be able to establish whether such effects will affect his particular system and to what extent.

The industrial implications of knowing how a high powered lasers will perform in an optical system are clear; it would mean higher beam quality, improved beam stability and better reliability. Which in turn would enable more data to be sent further down fiber optic cables, more steel to be cut per hour ,improve cancer treatment and make laser printing cheaper. In general it would enable the creation of better optical tools. With the rise in power of laser diodes it is envisaged that they could completely replace their expensive-bulky gas and solid state counterparts. This project is a small step on the way to improving the overall performance of high brightness laser diode systems.

2. Lasers

An overview of laser diodes and tapered lasers

This chapter has been included as an aid for readers whose area of primary expertise is not lasers, it covers some of the more fundamental principles of the Fabry-Perot laser and in the final stages tapered laser diode operation.

2.1 The principles behind the diode laser

The word laser is an acronym for Light Amplification by Stimulated Emission of Radiation. This describes quite accurately what a laser is. A source of highly directional coherent monochromatic light. The laser is based on the principle of stimulated emission. Unlike spontaneous emission, stimulated emission is a very fast process. The process is depicted below in Fig 2.1b, it shows an electron in the conduction

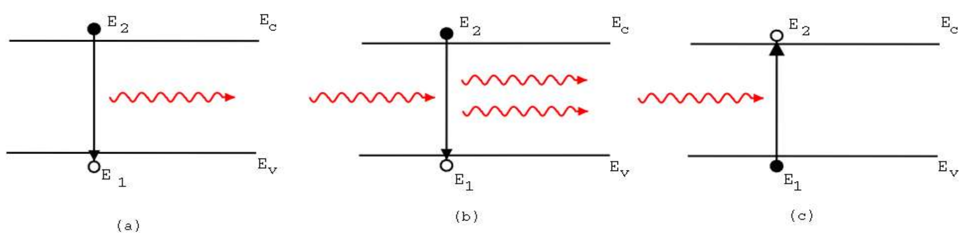

The processes of spontaneous emission, stimulated emission (b) and absorption (c). Figure 2.1

band with energy E_2, a photon from the left stimulates the electron in E_2 to fall in to a hole at energy level E_1. Assuming that this is a direct band gap semiconductor, a photon of energy $hf = E_2 - E_1$ will be lost in the fall. This photon will be of the same frequency, phase and direction as the photon which stimulated the emission. These two photons will stimulate more electrons to fall to the valance band, so that a large radiation field of monochromatic coherent light can be built up. Of course stimulated emission is not the only process at work inside of a semiconductor laser, spontaneous emission (Figure 2.1a) and absorption (Figure 2.1c) also occur. In a laser, these processes are undesirable as they give rise to non-coherent light and absorb photons, respectively. Spontaneous emission can be minimized by having a large photon field energy density, and we can ensure stimulated emission dominates over absorption by ensuring there are more electrons in the conduction band than in the valance band. This highly non-equilibrium state is called "population inversion".

The large photon field energy density can be encouraged by providing a resonant optical cavity, shown in figure 2.2.

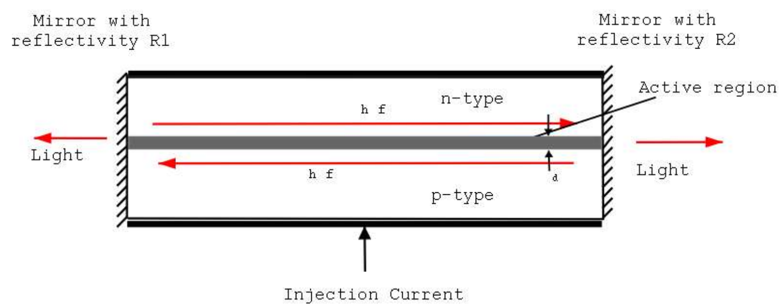

Figure 2.2a The laser cavity.

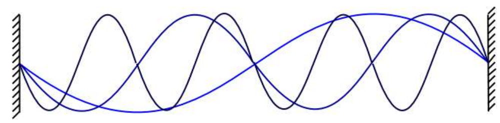

Figure 2.2b The lasers cavities supported modes its supported modes.

This cavity also performs frequency selection as any cavity does, it can only support certain modes, as illustrated in figure 2.2b. The energy difference between the modes can shown to be

$$\frac{\Delta E}{E}=\frac{\Delta f}{f}=\frac{c}{2\,lnf} \tag{2.1}$$

Of course the material does not give gain at every frequency. When one considers the inherent gain-loss characteristics of the material along with the frequency selection of the cavity, one finds that only a few modes are viable lazing modes. If one examines figure 2.3, it can be seen that the lasing modes only exist in the central region between the two vertical lines, where the gain exceeds the loss. The short spikes plotted at the bottom of the graph represent the wavelengths of the modes which the cavity can support. When one considers all these factors together, it becomes clear that the laser can only lase in a few modes. However it is not possible for all the modes to lase at once, as they compete with each other. The mode with most gain can stimulate more photons of its frequency than a mode with slightly fewer photons. The net result is that the mode with most gain will grow the fastest, taking electron-hole pairs in the gain medium away from the other modes. The result is that one mode dominates and its spectral width is far sharper than one would expect theoretically from such a resonant cavity.

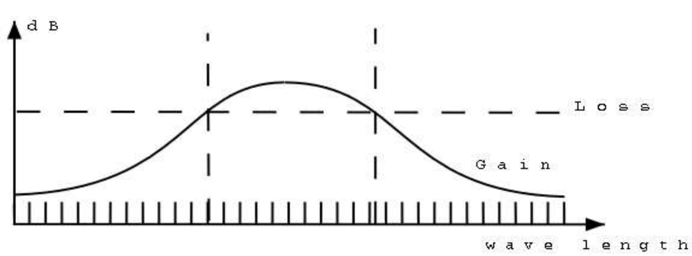

Figure 2.3 Viable lazing modes of the laser, the gain and loss curves have been shown along with the frequencies at which the cavity will resonate, denoted by the vertical lines on the horizontal axis.

Lasers are only useful if they emit light. It is therefore normal for one mirror of the resonant cavity to have a relatively high transmission constant and the other to have a relatively high reflectivity, so that light is radiated from only one end of the device. If one considers the gain, the loss and reflectivities of either end of the device, one can derive an equation (2.2) which relates these factors and must be satisfied in order for the laser to lase. In this equation $g(E)$ is the material gain per meter, Γ is the confinement factor (the fraction of the optical power in the active region), α_i is the material loss per meter L is the cavity length and $R_{1,} R_2$ are the power reflectivities of either end of the two mirror facets.

$$\Gamma g(E)=\alpha_i+\frac{1}{2L}\ln(\frac{1}{R_1 R_2}) \tag{2.2}$$

Population inversion must occur in order for the stimulated emission rate to be higher than the absorption rate. In a semiconductor laser this is achieved by applying an external voltage across the p-n junction. This reduces the built-in barrier which arises from negatively charged donors on p side of the junction and the positively charged acceptors on the n side, allowing electrons and holes to be injected across the barrier. Above a critical value of injection current, population inversion occurs, stimulated emission dominates absorption and the laser starts to lase. With out any quantum mechanical explanation, population inversion can best be described by considering equation 2.3

$$B_{21} f_2[1-f_1]>B_{12} f_1[1-f_2], \tag{2.3}$$

where B_{21} and B_{12} are the Einstein coefficients (which are equal), f_1, f_2 are the probability of an electron state at energy E_1 or E_2 being occupied respectively (see figure 2.1). Therefore, the probability of there being a hole in a state with energy E_1 or E_2 is given by one minus the probability of an electron being there. So, one can read the expression as the probability of, an electron being in the conduction band and a hole being in the valance band has to be greater than the probability of an electron being in the valance band and a hole in the conduction band. If one then replaces f_1, f_2 with the Fermi-Diac functions for E_1 or E_2 respectively,

$$f_2=\frac{1}{1+\exp(\frac{E_2-Fp}{kT})} \qquad f_1=\frac{1}{1+\exp(\frac{E_1-Fp}{kT})} \tag{2.4,2.5}$$

one gets after some manipulation the the expression $F_n-F_p>E_2-E_1$,which can be rewritten as $F_n-F_p>E_g$. Population inversion can therefore be understood as being when separation of the the quasi-Fermi levels for electrons and holes is greater than the band gap energy as shown below in figure 2.4.

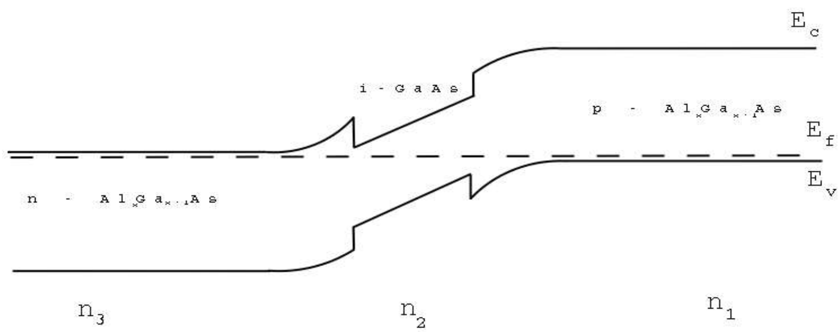

Figure 2.4a Energy bands at equilibrium in a hetrostructure laser,

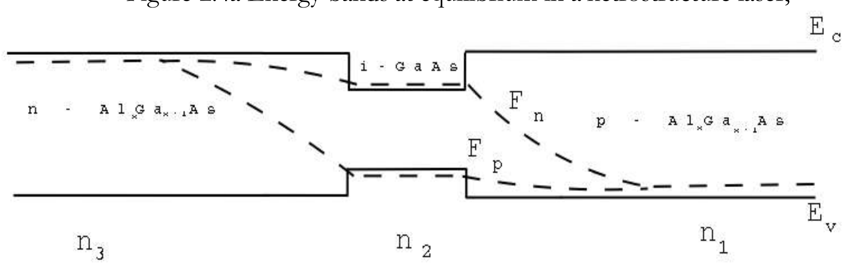

Figure 2.4b Energy bands in a lazing mode.

This brings us to our final point. If one examines figure 2.4, it can firstly be seen that the band diagram shows a hetrostructure and not an ordinary p-n junction. Secondly one sees that population inversion (i.e. $F_n - F_p > E_g$) only occurs within the intrinsic region of the diode. The hertostructure provides a means for electron confinement, which reduces the lasing area and thus the current required and the heat produced. Early lasers did not have this hetrostructure and could only be run in liquid nitrogen. A refractive index gradient ($n_2 \geq n_1 \geq n_3$) can also be introduced into the hertostructure to bring another advantage in terms of photon confinement. Modern lasers consist of five or more different materials used to create a quantum well in the order of 100Å and a waveguide of 100-1000nm.

2.2 Background on tapered laser diodes

A laser diode with a tapered gain region has been chosen for this set of experiments, these lasers have been shown to be capable of producing in excess of 3W of optical power [10], but it has been shown that they are especially susceptible to feedback effects when the back reflected light rises above the -30dB level[13]. This is in stark contrast to behavior of narrow stripe lasers. Therefore, it worth explaining a little about their internal structure.

This class of laser devices consists of two functional blocks, the ridge waveguide RW, and the tapered section. Their operation can be described as a master oscillator /power amplifier (MOPA), or an unstable-cavity. The ridge waveguide serves two purposes, firstly it provides a single spatial mode to the tapered section of the laser, and secondly, filters out radiation returning from the waveguide with spatial filtering. Due to practical limitations it is very difficult to generate large powers from the master oscillator [11]. Therefore, the tapered region must be capable of amplifying the small input power to produce a large output power. This is done by creating the taper out of material with a positive gain coefficient. The tapered shape causes the light propagation along the waveguide to diffract outwards, thus reducing its power density to reduces the risk of saturation and spatial hole burning, which cause effects such as self focussing and even filamentation. Reducing the power density also lowers the risk of Catastrophic Optical Damage [12] .

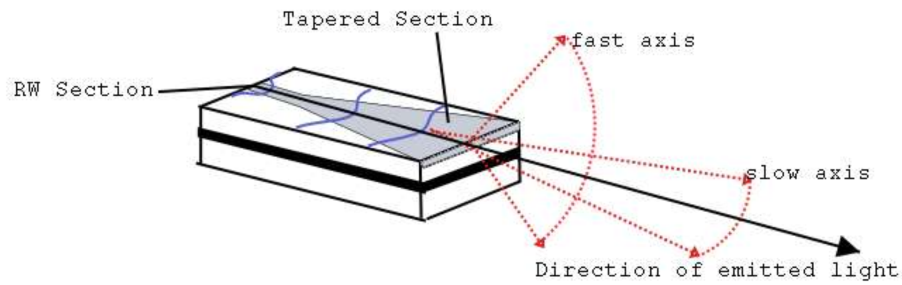

Figure 2.1, a pictorial example of light progressing down the structure of the laser and being emitted out the front. Note the astigmatic properties of the emitted light shown.

When the light reaches the wide end of the tapered amplifier most of it is radiated through the front of the device. That which is not (0.1%-1.5%) is reflected back in to the device where it continues to spread out. Thus most of the amplified back-reflected light does not couple back into the ridge wave-guide and may seed unwanted effects within the structure. The tapered shape of the wave guide improves the beam quality, but also hinders the development of corrective optics, because the propagated light forms an astigmatic beam (figure 2.1). When one examines the light from outside the laser in the slow access it seems to have a virtual source just inside the laser at a point given by Snell's law $n_1 \sin\theta_1 = n_2 \sin\theta_2$, which is approximately $\frac{L}{n}$ [11] where L is the length of the tapered section of the device and n is the effective index of the laser. In the vertical access, the beam appears from a virtual source on the end of the device. The two axes are normally refered to as the fast axis in the vertical direction (figure 2.1) and the slow axes in the horizontal direction. They are given these names because of the comparative rates of divergence of the light. In the the vertical axes the beam diverges very quickly however in the horizontal axes the beam diverges slowly. This is due to defecation. In the past, cylindrical lenses have been used to focus the light back into a non divergent beam.

3 The Laser Simulator - Conan

An overview of the Laser simulator and the modifications which were made to it

Before details of the interface the between laser simulator and the optical software can be discussed, it is first necessary to describe some aspects of the operation of the laser simulator. The detailed operation of the simulator can be found in other documents [14,38,39]. The following section aims to highlight in non-mathematical terms, the fundamentals needed to understand the operation of interface. The first section to this chapter will deal with the simulator and the second section will deal with the physical parameters of the device simulated.

3.1 The Laser Simulator

Conan is a state-state-of-the-art tapered laser diode simulator which performs *hot-cavity* simulations of high power tapered laser diodes. Hot-cavity simply means that the thermal equations are being solved along with the optical equations , resulting in a model capable of simulating nonlinear interactions resulting in effects such as spatial hold burning, filamentation, thermal lensing and optical pumping. Conan was built in a modular form with three key functional blocks, these are: The Thermal-Electrical Module ; the Control Module and the Optical Module (see figure 3.0). The Thermal-Electrical model is used to calculate the distribution of material gain and refractive index within the quantum well layers of the laser cavity. These distributions are passed to the electromagnetic model, which determines the propagation of the electromagnetic fields.

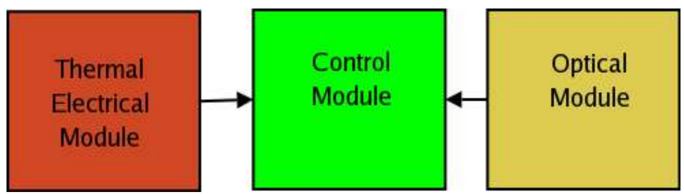

Figure 3.0 the modular structure of Conan

There are two ways in which the optical/thermal interactions can be treated; Firstly the entire photon distribution could be calculated for the entire cavity, these values then passed to the thermal module to be used to solve the electronic and thermal equations. The thermal module could then pass the carrier/temperature induced gain and index changes back to the optical solver for the entire process to repeat. This method is called the Separate Solution Method (SSM) and produces large culimnative errors in the photon distributions as the model does not take in to account the changes in the gain and refractive index as the fields propagate along the cavity.[14] The second method is called the Coupled Solution Method it is shown in figure 3.1. In this method, instead of running the optical/thermal modules in tern simulating the *entire* cavity, the cavity is split up into computational slices running across the cavity (see figure 3.1). The simulation starts at the back facet, where the initial forward propagating optical field is calculated using the fundamental mode of the ridge waveguide. The associated forward propagating photon distribution is passed to the thermal/electronic simulator which solves the electronic and thermal equations and calculates the associated carrier and temperature induced gain and index changes. This information is then passed to the next slice. This process of solving the cavity slices is continued until the front facet is reached, whereupon the optical field is multiplied by the reflection coefficient of the front facet mirror and the process of solving the optical/thermal slices starts again but this time traveling from the front facet to the back facet. This process continues until the field distribution, at the back facet converges. (see figure 3.2) Due to the computational intensity of solving the thermal/electrical equations, there are about 50-200 optical slices to every thermal slice. [14,38,39]

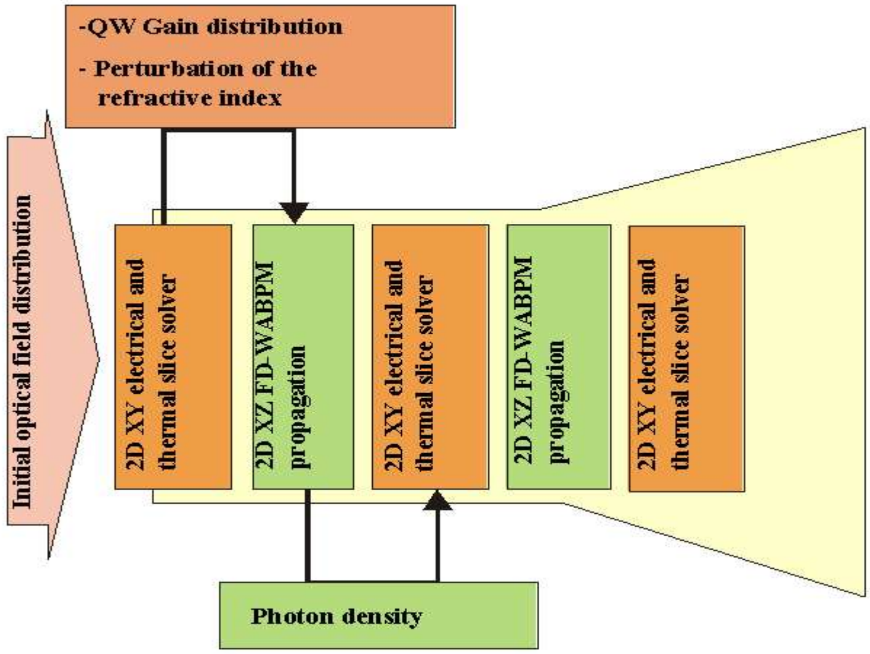

Fig 3.1 taken from Fig 2.2 [14] Showing a schematic illustrating the coupling of the electromagnetic and thermal/electrical modules using the coupled solution method to realize the hot cavity simulators

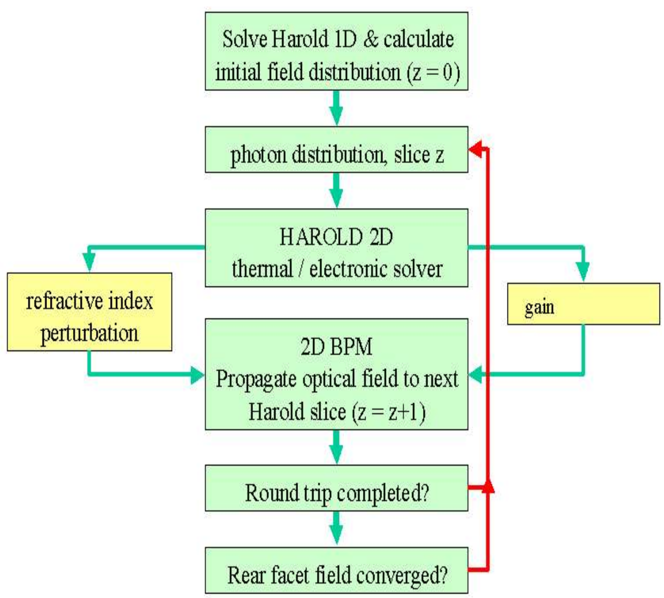

Fig 3.2 taken from Fig 2.2 [14] Demonstrates how the coupled solution method controls the transfer of information between the optical and thermal models.

As with any simulator which is designed to model the physical world, a certain number of assumptions have to be made, so that the problem can be solved with a reasonable amount of computational resources. Conan is no exception and there are three versions which perform three main types of simulation of varying accuracy to what would be physically expected. Of course, the draw back in performing a more accurate simulation is that it requires more time to run. Conan has been designed to perform three main types of simulation they are listed below:

<u>A half space 2.5D hot cavity simulator</u> This is a hot-cavity simulator which assumes symmetry across the optical axis of the laser cavity. This assumption means that only half the device has to be simulated as both halves of the device are considered mirror images of one another. This reduces the computational time by a factor of two. It consists of: a) 2D transverse electrical-thermal module, which solves the current continuity and heat conduction equations in half space; b) a 2D-WA-FDBPM optical module, which calculates the photon distribution in half space only; c) a control module, which employes the coupled solution method to control the flow of data between the optical and thermal modules; and a d) A viewer written in LabView, which is used to display the results of the simulation outputed periodically by the control module.[14]

<u>A full-space 2.5D hot-cavity simulator</u> This consists of a *full* 2D transverse electrical-thermal module, which solves the current continuity and heat conduction equations in the entire cavity (i.e a full space simulation – the device is no longer assumed to be symmetrical); b) a 2D WA-FDBPM optical module, which calculates the photon distribution in full space using the effective index approximation; and c) a control module which controls the flow of data between the optical and thermal module. (Note: no LabView visitation tool is available for this type of simulation)[14]

<u>A half-space 3D hot-cavity simulator</u> This consists of: a) a 2D transverse electrical-thermal module, which solves the current continuity and heat conduction equations in half space; b) a 3D WA-FDBPM optical module, which calculates the 2D photon distribution in half space; c) a control module to control the flow of information between the optical and thermal modules.[14]

It was decided that it was necessary do the modeling in a *full-space* simulation, because the back reflected light from the external optics may not be semetrical along the center of the cavity. This ruled out using any half space simulator, which also unfortunately ruled out using the 3D simulator. By not performing a full 3D simulation, other problems were introduced which will be explained later.

3.2 The modification of Conan

Conan is a very advanced laser simulator which has been under development for many years. However, no one previously had the need to couple third party optical software to it. This meant that there was no interface within Conan capable of outputing light from the simulator or receiving light from the 'outside world' during a simulation. Therefore such an interface had to be written. After assessing the structure of Conan (written in FORTRAN 90), it was decided that the best point to interface any software with it was as the numerical solver reached the front facet, the electric field could at this point quite easily be accessed. The interface would at this point have to write out the electrical field to a file and then wait for the back reflected light to be returned to the file. This back reflected light could then be read in by Conan and incorporated in to the solution of its equations.

It was felt that the most practical solution to carry the above out was to use three files: one file for Conan to output its electrical field; one file for the optical software to return the electrical field to Conan; and another file ,whose presence or absence could be used as a trigger to coordinate the execution of Conan and the optical simulation software. One entire simulation run will now be described from the point of view of Conan, it is also depicted in figure 3.3. Conan will be started as normal, it will initialize and start solving the cavity in slices, progressing along the cavity until the front facet has been reached. At this point it will write to disk a file called field1.out which will contain the electric field at the front the facet. Conan will then generate a file called 'go'. The generation of this file will be a signal for the optical simulator that Conan has produced data, which the optical simulator can work on. This file will then be read in by the optical simulator. The optical simulation software will then calculate the back reflected light from the optics, write out a file called field1.in. It will then delete the file 'go', which Conan generated. Meanwhile Conan, has been waiting for the file 'go' to be deleted. Once this has happened, Conan will know that the file field1.in is ready to be read, so it will read it in and replace the electric filed stored within Conan at the front facet by the one contained within the file. Conan will then use this new field and propagate the light back to the rear facet of the laser, reflect it off the back facet and propagate it once more back up to the front facet. At this point, the whole process of writing out field1.out and generating file 'go' will begin again. This whole process of passing data back and forth between the Conan and optical simulator will continue until convergence has occurred.

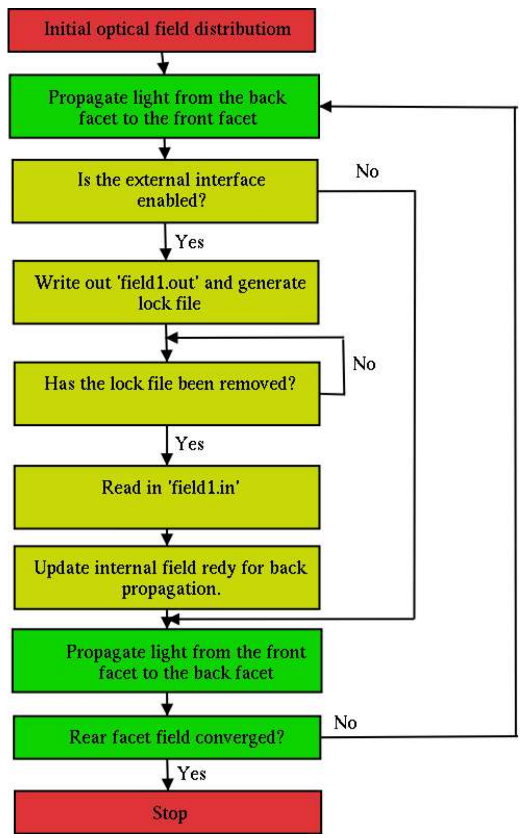

Figure 3.3 The execution of Conan, red green represents pre existing Conan code and yellow represents the new interface.

It was thought that one may still sometimes want to run Conan with out any external optics present. For this reason the external interface was placed in a Boolean conditional statement which if one sets to true, the new interface will run, and if one sets to false the new interface will not run. This is clearly visible in figure 3.3. *For the reference of those who wish to find both the statement and the interface, it is placed in conan01.f90 and the Boolean variable is called run_rods_section.*

The above is an accurate description of how the new interface within Conan works. However it must be pointed out that Conan never directly communicates with the optical simulator. There is a LabVIEW layer in-between the two simulators, which handles file conversion and synchronization of execution of the two simulators. This LabVIEW program requires its own chapter to be fully explained and will be presented later.

3.3 The structure of the simulated device

It was thought that the specific design of the device chosen for this set of experiments would have a large impact on the outcome of the experiment. One particular parameter which was of concern when choosing the device was the taper angle, as the larger the taper angle, the larger area of the front facet would be, this may make the device more susceptible to feedback.

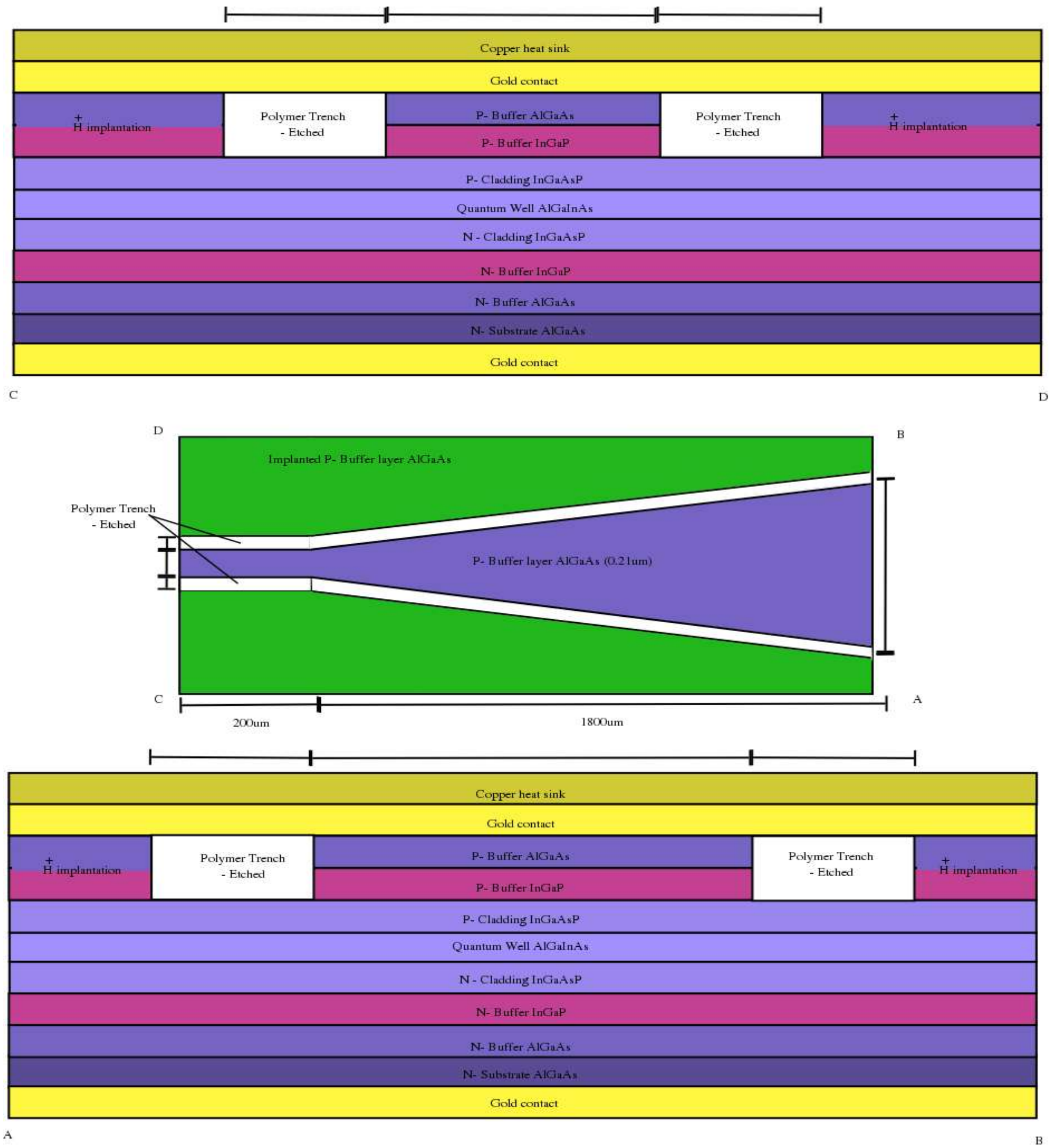

Figure 3.4 The structure of the device used through out the experiments the ridge wave-guide and tapered amplifier are clearly visible. Some dimensions have not been show for reasons of confidentiality.

After reviewing the relevant literature it was determined that nobody had before simulated and compared different device structures and their comparative susceptibility to external feedback. Therefore, it was quite hard to quantitatively choose a specific device for this set of experiments over another. It was however felt desirable to simulate a device which we possessed in the lab. This would give us the option of verifying the results later experimentally. Another factor considered was that the simulated device should not be too unusual in any way, by this it is meant that the simulated device should be well understood with no features which may hinder the analysis of the results. It was decided therefore to use an ordinary full index guided device with no beam spoilers as shown in figure 3.4, it has a relatively narrow taper ($<2^{o}$). This device provides optical confinement for the propagating light inside the taper by means of extending the etched trenches of the master oscillators along the length of the taper forming an extended ridge waveguide.

3.4 LabVIEW visualisation software - conversion to full cavity

In section 3.1, it was noted that software is available to display the results of the Conan simulations. This software is capable of plotting all the simulated parameters of the device including refractive index perturbation, photon density, material gain, p-contact current density, n-contact current density,hole densities, quasi-Fermi energy and local temperature of the quantum well, to name only a few. As Conan solves the device equations it saves its numerical solutions as it goes. The viewer software is able to display the output of the simulator in a pseudo dynamic manor. Unfortunately, however, the software was written at a time when Conan was only capable of performing half space simulations. Conan has since moved on to be able to do full space simulations. As this project will be using Conan in its full space mode, It was decided that viewer software must be updated to handle full space simulations, so that the results from the simulations could be fully examined. The software has three main components (one of which is not a viewer, it is a simulation editor). Each component's purpose and the modifications made to it are listed below. The component numbers assigned during K.L. Ooi project.

3.4.1 Component 1

Conan has a multitude of input files associated with it. These files are used to define material properties and device structure. Component 1 is designed to make the handling of these files easier. It presents the user with a mouse driven Graphical User Interface (GUI), with which the user can alter the configuration files. It somewhat guides the user through the process of configuring Conan with various help screens and comments. After some consideration, it was determined that this component did however not need altering as Conan has throughout its life cycle kept a good degree of backward compatability.

3.4.2 Component 2.2.1

This component is a viewer designed to display the results from a simulation as described above. It needed some modification in order to work for a full cavity simulation. The modifications were by no means wideranging. However, it took a considerable amount of time to understand the software to such a degree that one could have confidence in the changes which were made.

3.4.3 Component 2.2.2

This version of the viewer is a slight improvement Component 2.2.1. It is capable of comparing two sets of data from two independent simulations. It is very useful if one wishes to run two simulations with a parameter slightly altered and then compare the behavior of the model afterwards. Again, as the software was initially well written, it only needed slightly tweaking to make it compatible with the full cavity simulation output. Again, a considerable amount of time was spent understanding the software and then checking the changes, so that one could have confidence in them. A screen shot of Component's 2.2.2 GUI after the modifications were made is shown in figure 3.4.

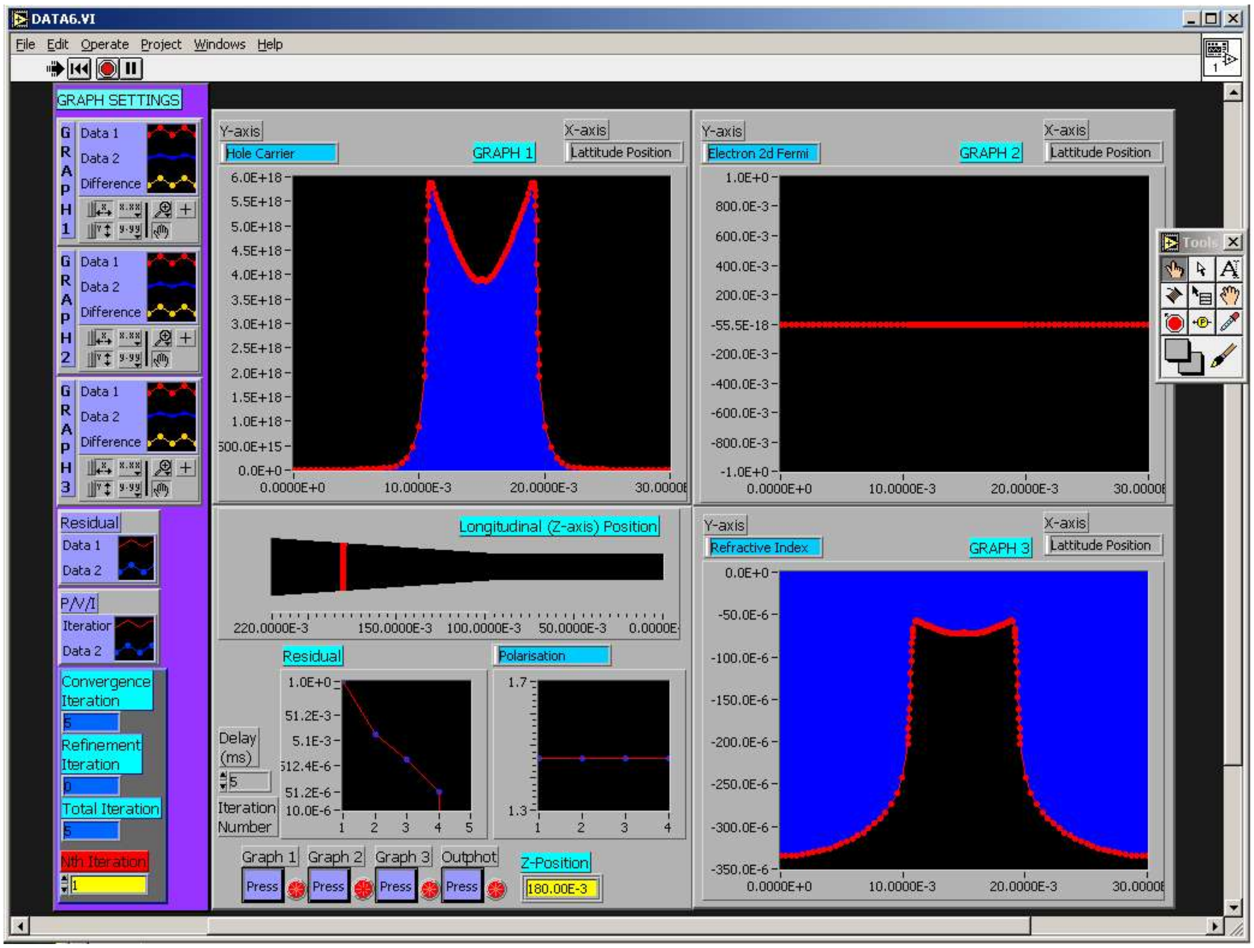

Figure 3.4 The updated visualization software

4 The Optical Simulation Software

A general overview of the optical simulation software and the development process.

4.1 Introduction

The original design brief of this project was to write an interface between ZEMAX. (an optical simulator) and Conan (a laser simulator). However, it turned out that ZEMAX was no longer available. Therefore, an optical simulator had to be created, which was capable of performing simple optical simulations including the simulation of mirrors with different reflection constants, simple lenses and most importantly of all, the ability to simulate the propagation of light in free space including the effects of diffraction. Diffraction is a very important phenomenon when considering laser behavior. One must consider that the laser's front facet ($1\mu m x 100\mu m$) has a size comparable to that of the wavelength of the light (0.975e-6m) it produces. Thus it is small enough to cause noticeable diffraction of the light which it generates. This of course is detrimental to the beam quality. The optical simulation software must be capable of taking the near field pattern just inside the front facet of the laser, propagating it to the optical components, simulating the optical components and then propagating the light back to the laser's front facet. Diffraction will play a major role in this and fortunately as J. Goodman demonstrates, the same equations can be used for the diffraction of light as for propagation in free space.[19] Once a solid foundation of diffraction has been built, it then becomes a matter of alteration of phase and introducing losses to represent most optical components.

There are two main approaches used to simulate diffraction. The first is the Rayleigh-Sommerfeld approach and the second is the angular spectrum approach. At the outset it was not clear which approach would be most successful. Therefore, two optical simulators were written during the course of this project. The first optical simulator was based on the Fresnel approximation to the Rayleigh-Sommerfeld equation. This produced accurate phase results past distances of about 4mm. However, at such close distances, the amplitudes of the peaks and troughs were only relative to each other, due to the assumptions made in the derivation. Therefore, it was decided to develop the second optical simulator based on the angular spectrum approach. This provided much better results - especially in the near field. In the this chapter, the principles of each simulator will be explained along with the advantages and disadvantages of each.

4.2 The Fresnel diffraction integral

Figure 4.1 shows plane light waves incident upon an object which extends for infinity in the horizontal and vertical axes. It has a small slit in its center. The light which falls upon the surface of the object is totally absorbed. The light which does not fall on the screen is propagated through the slit to a screen located a distance R away. The question now arises, what image does the light produce on a screen placed a distance R away.

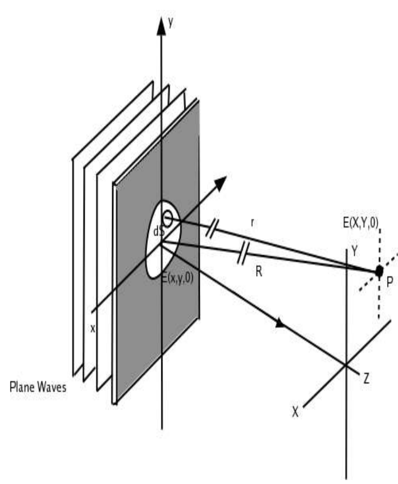

The amplitude per unit area of the waves incident on the slit is defined as $E(x,y)(amplitude/m^2)$. Appendix A shows that by considering the facet as comprised of many infinitely small areas, dS, which are essentially point sources normally termed Huygen wavelets, one can calculate the electric field at a point E(X,Y,Z). The mathematics presented assumes: a) that the electric field decays as the inverse of the distance propagated; and b) that by noting the distance from the point source dS to any point on the screen P, will vary across the screen. Therefore, by taking in to consideration the relative change of phase the light from every point source and summing the contribution of each source, one can calculate the light intensity at point P, and thus the over all diffraction pattern. Formula 4.1 is derived in Appendix A, where R is the distance to the screen, x,y are the Cartesian coordinates used to define the aperture, X,Y are the Cartesian coordinates used to define the position on the image screen, λ_o is the wavelength of the simulated light, and $k_o=\frac{2\pi}{\lambda_o}$ which is called the propagation constant of the medium. It is assumed that $\lambda=\frac{\lambda_o}{n}$ where λ is the wavelength of the light in the free space, and n is the refractive index of the medium.

$$E(X,Y)=\frac{e^{jk_o R}}{j\lambda R}e^{j\frac{k_o}{2R}(X^2+Y^2)}\sum_{x=-\infty}^{\infty}\sum_{y=-\infty}^{\infty}\{E(x,y)e^{\frac{-jk_o}{2R}(x^2+y^2)}e^{-j\frac{2\pi}{\lambda R}(Xx+Yy)}\} \tag{4.1}$$

A C program was written to implement formula 4.1. It is capable of reading in an ASCII file containing complex numbers. The program takes this as the input field E(x,y). It then applies the above formula for every E(X,Y), to generate the diffraction pattern on the screen at distance R. The program then saves this resultant field back to a file.

4.3 Results from the first optical simulator

Some results generated from the optical simulator will now be shown. The results are taken from a series of tests which were run on the simulation software to validate its results with known results taken from books [15]. Fig 4.2 shows the result given by the laser simulator when the near field pattern from a Conan test run is placed as an input to the optical simulation software. Fig 4.2a represents what would be seen if a tiny screen were placed $10\mu m$ meters away from the laser front facet of the exactly the same dimensions as the laser facet. The first peak and the first two troughs can clearly be seen. At the edge of the graph at 0 and 1e-5 on the slow access the curve starts to rise up and form what would be the second peaks.

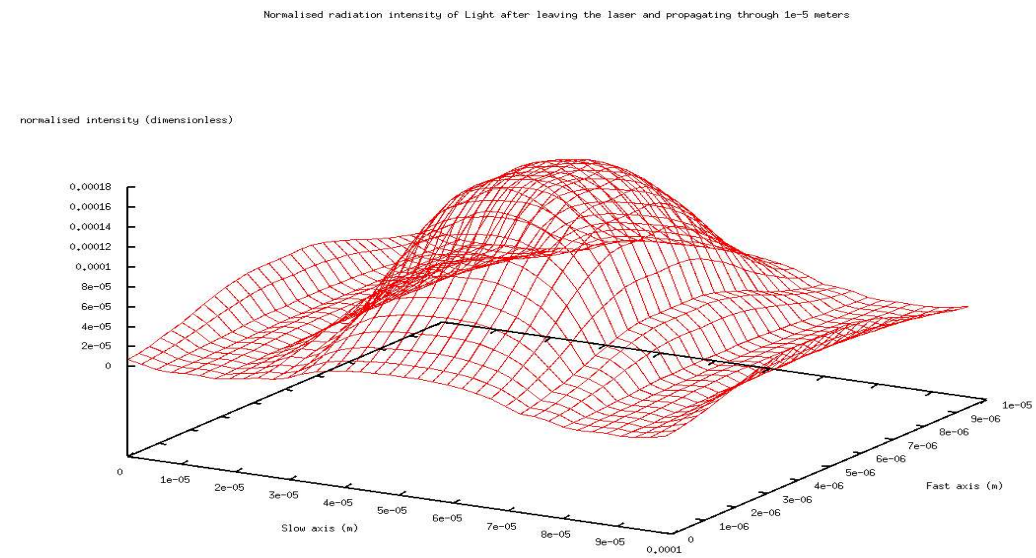

Fig 4.2a The normalized near field of the laser (taken at a distance of $10\,\mu m$ with a total area of $10\,\mu m\,x\,100\,\mu m$)

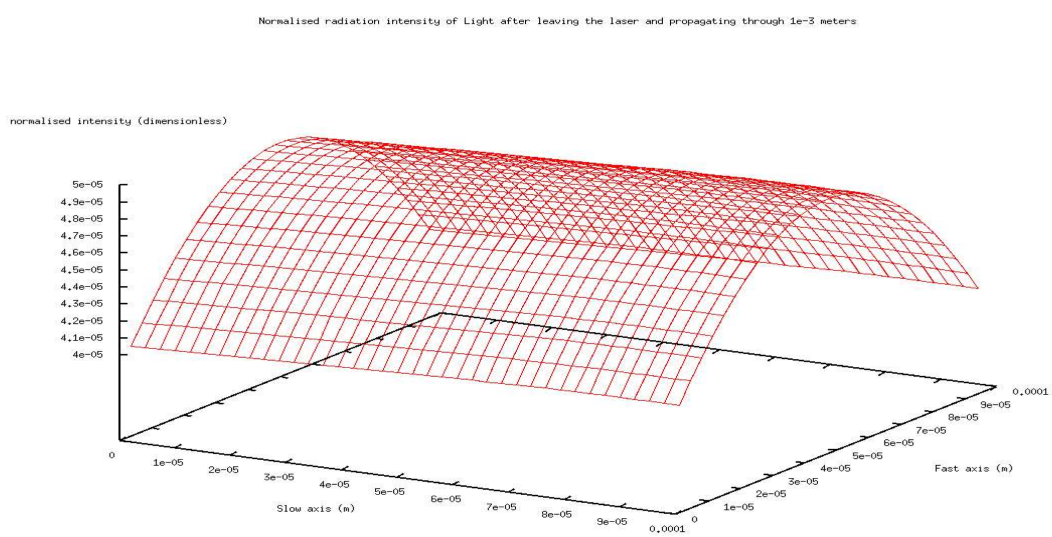

Fig 4.2b The normalized near field of the laser (taken at a distance of 1mm, with a total area of $100\,\mu m\,x\,100\,\mu m$)

Figure 4.2b shows a $100\,\mu m\,x\,100\,\mu m$ screen placed 1.0mm in front of the laser. What one would theoretically expect from such a simulation of a slit which was very narrow in one axis (fast) and very wide in the other axis (slow) would be a very slowly varying diffraction pattern in the slow axis, and a rapidly varying diffraction pattern along the fast axis. This is clearly visible in figure 4.2a, (when viewing this diagram one must note the scales - the slow axis scale is ten times larger than the fast axis scale. The other effect one would notice would a spreading out of the beam as one moves away from the source. This spreading out would result in slower change of field with respect to both the slow and fast axes. If one examines figure 4.2b, this effect can be seen. All these results concur with theory.

4.4 An estimation of the accuracy

According to Goodman[19], the phase and thus the relative intensity holds for a distance R away from a slit in such that the following relation is satisfied:

$$R^3 \gg \frac{\pi}{4\lambda}((x-\xi)^2+(y-\eta)^2)^2$$

(4.2)

$$E(X,Y)=\frac{e^{jkR}}{j\lambda R}e^{j\frac{k}{2R}(X^2+Y^2)}\iint_{-\infty}^{\infty}\{E(X,Y)e^{\frac{-jk}{2R}(x^2+y^2)}e^{-j\frac{2\pi}{\lambda R}(Xx+Yy)}\}\,dx\,dy$$

(4.3)

where x is half the maximum slit width of the laser, y is half the maximum laser height, ξ is half the horizontal maximum observation distance from the center of the projected image and η is half the vertical maximum observation distance from the center of the projected image. For a typical tapered laser, it results in a distance of about 4mm. However, there is a another problem in the derivation. It is assumed that radiation drops off inversely to the distance from from the slit, this assumption holds for distances far from the slit, but when $R \ll 1$ the amplitude of the resultant electric field becomes unrealistically large. This can be seen by examining equation 4.3 (the integral from of 4.1) and observing that as $\lim_{R\to 0} E(X,Y)\to\infty$. This proved very problematic - especially in the near field region.

The Second Optical Simulator based on the Fourier transform.

4.5 Theory [18][19]

It is possible to develop diffraction theory in a different way. One can use a framework which closely resembles the theory of linear systems. If a monochramatic disturbance is Fourier analyzed across any plane one may think of the various spatial Fourier components as plane waves traveling away from the plane. One may then propagate this plane to a destination plane by taking in to account the various phase shifts associated with the propagation of the various plane waves. If one then inverse Fourier transforms the light, one gets then the final image.[18][19] If one considers the slit in Fig 4.1 again, the Fourier transform of the electric field incident upon the aperture can be written as

$$A(f_x,f_y;0)=\iint_{-\infty-\infty}^{\infty\,\infty} E(x,y,0)\exp[-j2\pi(f_x x+f_y y)]\,dxdy$$

(4.4)

and its inverse Fourier transform may be written as

$$E(x,y;0)=\iint_{-\infty-\infty}^{\infty\infty} A(f_x,f_y,0)\exp[j2\pi(f_x x+f_y y)]df_x df_y$$

(4.5)

To underline the physical meaning of this equation, one may consider the exponential part of the integral as being a plane wave propagating through space. A wave such as this is represented by the equation

$$p(x,y,z;t)=\exp[j\boldsymbol{k}\cdot\boldsymbol{r}-2\pi vt] \quad ,$$

(4.6)

where k is the direction of propagation such that

$$\boldsymbol{k}=\frac{2\pi}{\lambda}(\alpha\hat{x}+\beta\hat{y}+\gamma\hat{z})$$

(4.7)

and r is the position vector

$$\boldsymbol{r}=(x\hat{x}+y\hat{y}+z\hat{z})$$

(4.8)

Removing the time variance term, one gets the expression

$$p(x,y,z)=\exp[j\boldsymbol{k}\cdot\boldsymbol{r}]=\exp[j\frac{2\pi}{\lambda}(\alpha x+\beta y)]\exp[j\frac{2\pi}{\lambda}\gamma z]$$

(4.9)

where

$$\gamma=\sqrt{1-\alpha^2-\beta^2} \quad .$$

(4.10)

Thus one can rewrite the Fourier transform kernel with

$$\alpha=\lambda f_x \qquad \gamma=\sqrt{1-(\lambda f_x)^2-(\lambda f_y)^2} \qquad \beta=\lambda f_y$$

(4.10,4.11,4.12)

as

$$A(\frac{\alpha}{\lambda},\frac{\beta}{\lambda};0)=\iint_{-\infty-\infty}^{\infty\infty} E(x,y,0)\exp[-j2\pi(\frac{\alpha}{\lambda}x+\frac{\beta}{\lambda}y)]dxdy$$

(4.13)

This is called the angular spectrum of the disturbance $E(x,y,0)$ of . The problem still remains how to propagate the angular spectrum from $A(\alpha/\lambda,\beta/\lambda;0)$ to $A(\alpha/\lambda,\beta/\lambda;z)$. One may do this with the following method:

For values of $\alpha^2+\beta^2<1$, one may assume

$$A(\frac{\alpha}{\lambda},\frac{\beta}{\lambda};z)=A(\frac{\alpha}{\lambda},\frac{\beta}{\lambda};0)\exp[-j2\sqrt{1-\alpha^2-\beta^2}\cdot z]$$

(4.14)

and when $\alpha^2+\beta^2>1$

(4.15)

$$A(\frac{\alpha}{\lambda},\frac{\beta}{\lambda};z)=A(\frac{\alpha}{\lambda},\frac{\beta}{\lambda};0)\exp(-\mu z) \tag{4.16}$$

where

$$\mu=\sqrt{(\lambda f_x)^2+(\lambda f_y)^2-1} \tag{4.17}$$

Thus, to propagate the angular spectrum $A(\frac{\alpha}{\lambda},\frac{\beta}{\lambda};0)$ through a distance z, one may use 4.14 to change the relative phase of the components of the angular spectrum in accordance with the distance propagated. However, when 4.15 is satisfied, the angular components are attenuated according to 4.16. This attenuation is analogous to evanescent waves in waveguides.[19] The above mathematics is a shortened version of what appears in J. Goodman's book [19] p57, he explains the mathematics in more detail and it is highly recommend reading for anyone wishing to continue this work.

4.6 The implementation of Fourier diffraction in software [18][19][44]

The above mathematics is a far more accurate way to simulate the propagation of light and indeed its diffraction. It produces far better results - especially in the near field. To implement it in a computer ,program firstly the 2D Fourier transform of the input light. In our case the electric field leaving the laser i.e.,

$$E(x,y;0)\rightarrow A(f_x,f_y;0) \tag{4.18}$$

Next, the the correct phase shift must be applied in order to propagate the light the desired distance. The phase shift function is represented by $H(f_x,f_y;z)$

$$A(f_x,f_y;z)=A(f_x,f_y;0)H(f_x,f_y;z) \tag{4.19}$$

The inverse Fourier transform is then applied to recover the diffracted electric field.

$$A(f_x,f_y;z)\rightarrow E(x,y;z) \tag{4.20}$$

And of course $H(f_x,f_y;z)$ is defined as

$$H(f_x,f_y;z)=\begin{cases}\exp[-j2\sqrt{1-\alpha^2-\beta^2}\cdot z] & \text{if } \alpha^2+\beta^2<1\\ \exp(-\mu z) & \text{if } \alpha^2+\beta^2\geq 1\end{cases} \tag{4.20}$$

The Fourier transform was implemented by an FFT algorithm supplied by Numerical Recipes (www.nr.com) in C. C was used for this application because of its efficient ability to handle memory and to do fast calculations. This software was developed and demonstrated to be accurate.

4.7 Problems with the implementation of the FFT

The way Conan represents the light leaving the front facet is not straight forward but for the time being it can be taken that the light emitting region typically measures about $4\mu m \, x \, 50\mu m$ meters, and is represented by a (50x250) two dimensional array of complex numbers. It was decided desirable that the data coming back from the optics should be at the same definition as the light leaving the laser. That is to say that it would not make any sense to return an array from the optics with 100x500 data elements, as the laser simulator could not accept all these data points and it would therefore waste memory. In the same way it would not make sense to return a 4x4 array of data points to the laser as accuracy would be lost. Stipulating this match of resolution is fine in an ideal world. However, due mainly to diffraction, the further light travels from an optical source the more the light will spread out. This has very serious consequences for optical simulation software, as the more the light spreads out (by applying 4.19), the more memory is required to simulate the screen on which the light falls. One of the assumptions made when using a Fourier transform is that the sampled signal is assumed to be periodic. This means 'images' (copies) of the signal will appear in all directions for for infinity. This in its self is not a problem, however as light diffracts as it spreads out, this means that all the images of the light signal will also spread out, and at some point will start to interfere with each other. The position of the image signals are given by 4.21.

$$E(x,y)=E(x+NX,y+MY) \tag{4.21}$$

where N is the number of samples along the horizontal axis, M is the number of samples along the vertical axis and X,Y are the image numbers in the horizontal and vertical axes respectively. Therefore we can say that if the image spreads by over N or M pixels then the images will start to interfere with one another and the 'banding' visible in figure 4.3 will occur.

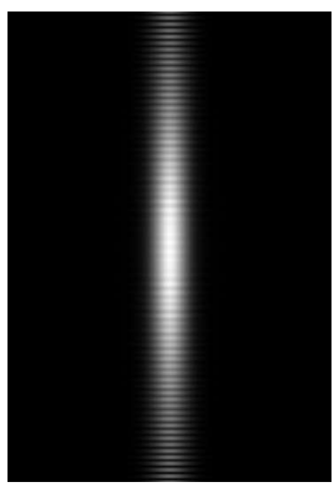

Fig 4.3 an example of interfering images, the 'bands' produced by overlapping images are clearly visible at the top and bottom of the figure. This figure shows the diffracting light coming out of a laser whose horizontal (slow) is aligned along the horizontal axes of the image and fast axes aligned the vertical axes of the image. What is especially interesting about this figure is that the images are only interfering in the vertical axes this is because of light coming out of the laser diverges faster in the vertical axes than the horizontal axes.

The simple solution to this problem is to make the 'screen' (output array) bigger, so that the images do not interfere with each other and the banding is avoided. This is a good idea in principle, however some simple arithmetic shows that it would require about $57\,Tbytes/m^2$ to represent a one meter screen at this data resolution. In fact this was the approach used, but it meant that one had to be very careful to limit the propagation distance. One could also manipulate the vertical resolution, as Conan only used 2D BPM (Chapter 5). However, again one had to be quite careful. An average simulation required a little over 500Mb of physical memory to run.

Another problem with this method is that one only requires a very tiny section of the back reflected image. For example, if the light from a laser is emitted from an area of $4\mu m x 100\mu m$ and the light propagates through 1cm spreading to an area 0.5cm only about $4\mu m x 100\mu m$ of the light can link back in to the laser. This which means that 99.9992% of the calculated image and thus the calculation time and memory are not used. That is one of the key reasons the Fresnel simulator (the first approach) was developed, as it was thought that it may firstly save memory/calculation time, since one may calculate only the required points to the desired resolution, however the FFT based simulator produced better results if used with care.

4.8 The architecture of the Optical Simulator

The nucleus of the optical simulator has been described in sections 4.5-6. This section will expand on details of this program focusing on interfaces, file formats and the specifics of operation. By doing this, it is hoped to give someone who may wish to continue this work a good understanding of the optical simulator and enable them to quickly use or modify it.

The operation of the laser simulator will now be described from the programs execution to its termination. The optical simulator accepts the input file, the output file and its configuration file as command line arguments. This will enable easy integration into other software and scripts. See fig 4.3 and example of how to call the optical simulator from the command line.

./OptSim input_file output_file config_file

Fig 4.3 The arguments the optical simulator accepts, where input_file is a text file containing complex number representing the electric field leaving the laser and the output file is the filed after having passed through the optical simulator and the config_file is a configuration file used to pass options to the optical simulator.

Once executed, the first things the laser simulator needs to know before it can apply any of the mathematics presented in section 4.6 are the dimensions of the input field, the dimensions of the output field and the distance by which the light must be propagated. The optical simulator aquires this data from the configuration file. The configuration file has the following file format.

```
[input]
width=100e-6
height=4e-6
width_data_points=250
eight_data_points=50
[output]
width=1e-3
height=1e-3
[prop_dist]
distance=1e-3
```

Once this file has been read, the simulator then reads an ASCII file containing a 2D array of complex numbers representing the input field. After the optical simulator has finished reading these two files, it has all the information needed to run the simulation. The file representing the input field should be arranged as shown in figure 4.4. Between each column, there should be a space (ASCII 20H). At the end of each row, there should be a carriage return (ASCII 0DH).

Vertical axis		1		2		3		..n
Horizontal axis	Re	Im	Re	Im	Re	Im	Re	Im
1	X	X	X	X	X	X	X	X
2	X	X	X	X	X	X	X	X
3	X	X	X	X	X	X	X	X

4.4a

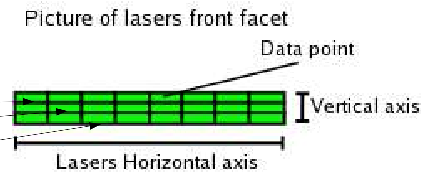

4.4b

Figure 4.4a represents the file format of the input file accepted by the optical simulator representing the complex input light, Figure 4.4b represents the digitized input field (possibly from the laser's front facet), one could imagine it being a section of the lasers front facet, with the observer looking straight at it. The arrows going between the two pictures show which complex number in the file correspond to the input field from the optical source.

When reading the above section one could be forgiven for thinking that the above array is read straight in to a simple complex 2D array of exactly the same dimension as the data contained within the input file. However, when one considers that the light will spread as it propagates (section 4.7), it becomes clear that the data must be placed in the middle of a very large array. This array must be large enough to still contain all the simulated light within its boarders after propagation has been accounted for in order to avoid problems with imaging. As the program starts, one of its first jobs is to define an array with the same resolution as the input array, but of size as defined in the configuration file as the output file. The simulator then reads in the input field and places the data at an offset (i.e in the middle) of this very big newly generated array. The Fourier transforms have been chosen so that they operate on an array and store the result in the same array. This saves memory, so after propagation has occurred, this very small input field placed in the middle of this very large array, will be transformed in to the propagated light covering the entirety of the array.

By this stage, the program should have calculated the propagated light. The obvious thing to do would be to save the field straight to disk, ready to be accepted by the laser simulator. However, there is no point in saving the entire array to disk, because it would require over 2Gb of disk space and not all of the diffracted light is able to be accepted by the laser. If one considers that the lasers front facet measures only about $4\mu m x 100\mu m$ and the light may have diffracted out to $1 mm x 1 mm$ there is no chance all of that light can reenter the facet as it would simply not be incident upon it. Therefore, we assume that only the region which emits light from the front of laser can accept back- reflected light, so the optical simulator extracts a the tiny region out of the output image which corresponds to the light which could be accepted by the laser. This reduces the 2Gb of data file to a few tens of kilobytes.

The output field is stored in a text file in exactly the same format as the input field. In order to assess the accuracy of the simulation and to pick up on any errors (a typical error would be to rotate the input field by 90 degrees or to have missed out a minus in an exponent so the light propagated the back in to the laser), the optical simulator creates several pnn image files during the simulation. Pnn files are relatively simple image files which contain no compression and no pallet information there format is as described in table 4.1.

Start offset	Item Length	Data	Example
0	3	P6+"carriage return"	P6\n
3	X	"Image width"+"space"+ "Image height"+"carriage return"	260 250\n
X+3	3	"R"+"G"+"B"	0Dh0Ah0fh
X+6	3	"R"+"G"+"B"	0Dh0Ah0fh
....	3	....	...
X+3*(Image width)*(Image Height)	3	"R"+"G"+"B"	0Dh0Ah0fh

Table 4.1 an example of a ppn

The section of code used to generate files of this type is shown below:

```
int image = open("/rod/image.pnn", O_RDWR|O_CREAT);
sprintf(temp, "P6\n%d %d 255\n", win.width, win.height);
write(image,temp,strlen(temp));
write(image,buffer,win.width*win.height*3);
close(image);
```

This type of file can be read by any reasonable image viewer (GIMP/Paint Shop Pro). As with any type of bitmap, it saves data using three eight bit bytes representing the red, green and blue components of a pixel. This meant that the two thirtytwo bit floating point numbers used to represent the real and complex field components had to be normalized to 8 bit numbers. As no complex measurements were going to be taken from the image files and they were only going to be used as a check on the progression/performance of the simulation, it was decided to save the normalized (on to $2^8(255)bit$) modules of the data. Four different images are generated during the simulation process, a typical example of such the images is shown below in figure 4.5. Figure 4.5.a is an image of the input light once it has been read in and positioned in the data array. One can use this image to check that the optical data has been read in correctly, that it is of the correct orientation and that is has been centered in the middle of the image correctly. Once the FFT has been completed another image is created figure 4.5.b. This image has as of yet not been used, but it is there for completeness. Then once the inverse FFT has been completed, two images are created - one with the full image of the diffraction pattern at distance z (figure 4.5.c) and another one only this time covering only the area of the light saved in the 2D output array (figure 4.5.d). This is to check that the optical simulator has cut the correct section out of the diffracted image, which will be incident on the front facet.

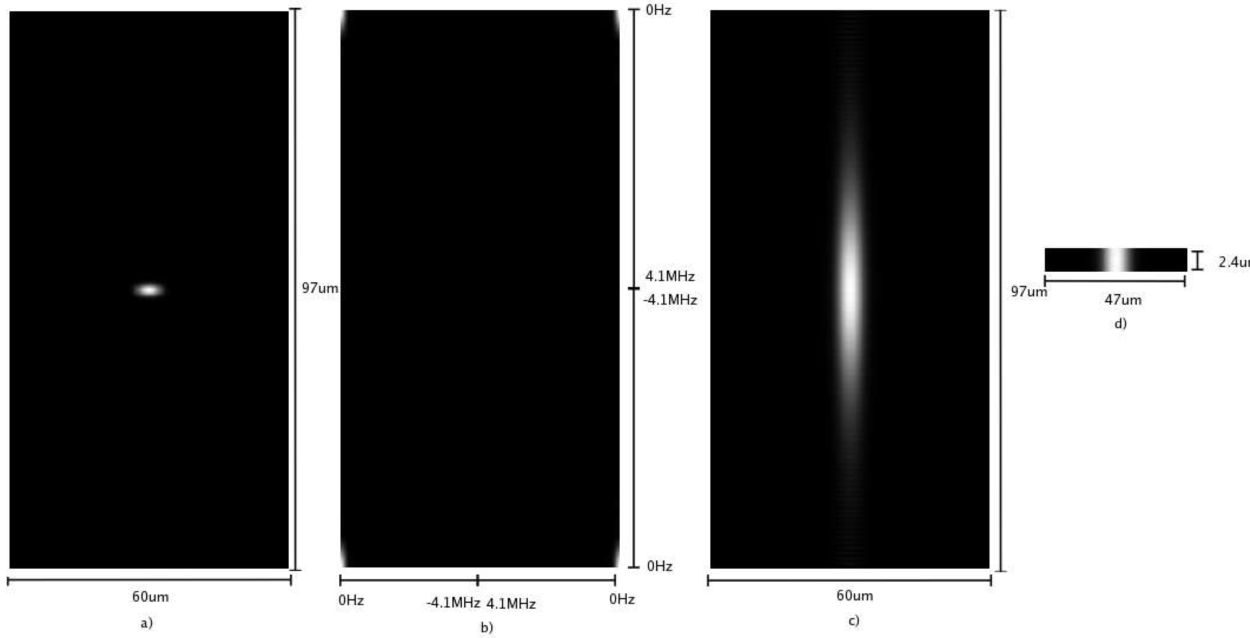

Figure 4.5 This is a simulation of a tapered laser. a) The input optical field superimposed on a black background with lots of padding around the edges to project against banding at z=0. b) The FFT taken at z=0, shows spatial frequency, the way the scales are arranged is stipulated by the operation of the FFT algorithm. c) the propagated light 20 wavelengths (0.975nm) away from z=0. d) the small image is the optical data which was cut out of the final propagated field read to be processed by the Conan optics interface.

Tapered lasers typically produce an asymmetric beam with a divergence of $20-45^o$ along the fast axis and $6-20^o$ along the slow axis. This spreading of the beam is used as a rough comparison of beam quality for lasers. It could also be used to verify the operation of the optical simulator. The divergence of the beam is calculated with simple geometry by calculating the angle from the edge of the spread beam in the far field to the center of the laser's facet. However, in order to calculate this angle, one needs to define the beam's edge in the far field. This is done normally done by using the $1/e^2$ point or sometimes the 3dB point. In order to aid in the calculation of the divergence angle, the simulator was given the ability to indicate the 3dB/ $1/e^2$ points in the output pnn files with false color. An example of such an output file with false color is shown below in figure 4.6.

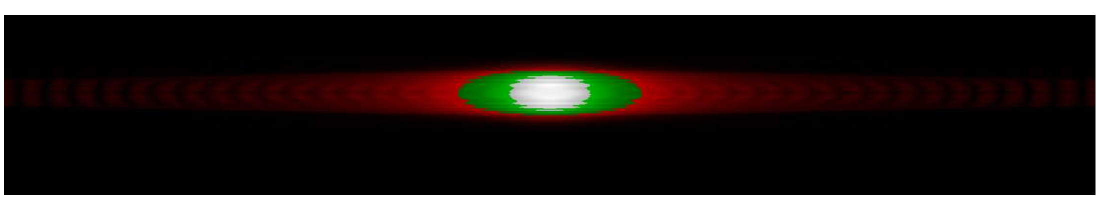

Figure 4.6 An example of false coloration to signify the 3dB/ $1/e^2$ points, the interface between the green and red signifies the $1/e^2$ point and the interface between the white and the green signifies the 3dB point.

A simulation often takes up to ten minuets to run. Therefore, a percentage count of the completeness of the calculation is given. This can also be used to check if the calculation has stalled for some reason. Versions were compiled for for both the PC (Windows, Linux) and Compaq Workstations (True Unix 64).

4.9 Mirrors and dielectric interfaces

The propagation of light through air is a linear process and the reflection and transmission of light is also a linear process. Therefore if one wishes to place a mirror with a certain transmission constant in the system, it does not matter much where one places this mirror. For example, suppose one is simulating a mirror as a perfect conductor at distance d from the laser. In this case one could propagate the light a distance 2d , i.e. to the mirror and back to the laser, then take account for the phase change and any other factors later. In fact this is what is done, as it reduces the number of instructions executed in the software by a factor of two. We have already developed software to propagate the light through space. This section discusses how the propagated light must be altered to simulate a variety of optical components.

4.10 Software

It would have been a simple matter to place various functions and procedures within the C program, to enforce the boundary conditions required for the simulation of optical components. However this would mean that every time a new optical system was implemented, the C program would have to be recompiled. Also, not everybody who wishes to use the software can program in C combined with the fact that no complex mathematics will have to be performed to simulate the optical components. It was therefore thought better, to separate the simulation of the optical components from the optical simulator itself. The memory intensive simulation of propagation and diffraction will remain in a C program, but the simulation of the components themselves will be written in LabVIEW, in effect a LabVIEW optical simulator will be made, which has an interface to a highly optimized C program capable of simulating the propagation of light.

4.11 A perfectly conducting metal plate and other things – outside Conan

Let us consider a uniform plane wave incident on a perfectly conducting metal plate. One can write the summation of the incident $E_+ e^{-jk}$ and reflected $E_- e^{jkz}$ waves as

$$E_x(z) = E_+ e^{-jk} + E_- e^{jkz} \tag{4.22}$$

if we set z=0 at the metal plate and consider that the total field must equal 0 as required by a perfect conductor, $E_x(0)=0$. We can then write $E_- = -E_+$. So the required transformation to our light propagated by our optical simulator is to flip the phase and multiply the field by -1. This principle can be generalized and the amplitude of forward propagating wave linked to that of the back propagating wave by defining a reflection coefficient ρ (equation 4.23) [20], where Z_L is the impedance of the mirror and η is the impedance of free space.

$$\rho = \frac{E_-}{E_+} = \frac{Z_L - \eta}{Z_L + \eta} \tag{4.23}$$

However, this is not in a very useful form as the impedances of glasses are hard to find in books and catalogues normally use refractive indexes. The equation can be rewritten in terms of refractive index as long as the permeability of both mediums is the same. (Clearly, the equation no longer holds for metals)

$$\rho = \frac{E_-}{E_+} = \frac{n_2 - n_1}{n_1 + n_2}$$

(4.24)

A Labview vi (roughly to a function in C) was written to implement this. This vi is shown below in figure 4.7. It simply takes the input field as an array and outputs the array after flipping the phase and applying the above formula.

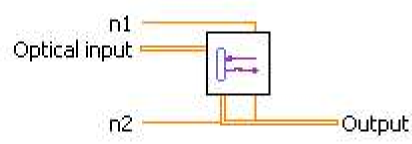

Figure 4.7 A LabView vi

4.12 Mirrors inside Conan

Conan does not take in to account phase reversals off its own mirrors as all phase is relative within Conan. However for my software it is very important to keep track of the phase, as the back reflected light must be added to the reflected light off Conan's mirrors making the phase very important. What this means is that for every time the light bounces off a mirror outside of Conan there must be a 180 degree phase flip. However, when simulating mirrors within Conan, there is to be no phase flip. With the external interface engaged within Conan, LabView takes over the responsibility for the front mirror facet of the simulated laser. Therefore, it is also important that there is a component which can simulate a mirror without a phase flip. Such a component was written and is called mirror.vi. It is shown below in figure 4.8

Figure 4.8 A vi that simulates a mirror in side Conan

4.13 The optical simulation system

Here the optical simulation system within LabVIEW can be seen in its assembled form. Each component has been designated a number to help with this description. Component 1 will be described later. It is an interface with Conan to retrieve the front facet reflectivity from one of the configuration files. Component 2 simulates the transmission factor of the front mirror of the laser twice as the light must go through it twice, (once on the way out and once on the way back in). Then the data is passed to the optical simulator component, which alters the phase and amplitude of the returning light in accordance with the object which is being simulated. In this case a BK7 glass-air interface is being simulated at 975nm. Hence n1=1 and n2=1.51. In a real system, a 2D array of complex numbers representing the field coming from the optical simulation software would be inputed in to the first mirror component (2).

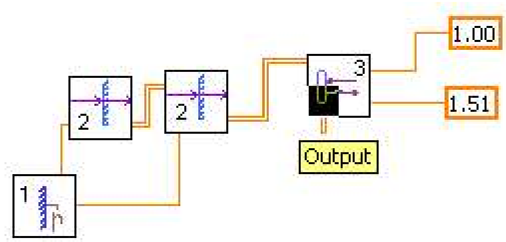

Figure 4.9 A screen shot of the assembled lab view components,

which simulate the mirrors in side and out side of Conan

5. The Overlap Principle

The calculation of the overlap between light incident on the laser's front facet and the fundamental vertical mode of the laser cavity.

5.1 The reason for this calculation

Conan uses the 2D finite difference beam propagation method (FD-BPM) [29,30] to simulate the propagation of electromagnetic waves within the laser's optical cavity. BPM is widely use to simulate structures not having translational symmetry, such as couplers, tapers and bends. It allows the propagation of eigenmodes within a wave-guide[31]. BPM has been in use since the late 1970 when it was used for simulation of light propagation in fiber optics systems. The early algorithms were based on discrete Fourier transformation (FT-BPM). Since this time, other methods have been developed including the line method (Mol-BMP), the finite element method (FE-BPM) and of course finite difference BPM. There are several analytical implementations of this algorithm including 1D BPM, 2D BMP and 3D BPM. All of these methods assume the forward propagation of the electromagnetic wave within the cavity and solve the device equations starting at the back facet and move towards the front with out considering reflections. Once the front facet is reached, the process continues only starting this time at the front facet and moving towards the back facet. Once one full pass is completed, convergence is checked for and if the solution has not converged the round trip is repeated until convergence occurs (see chapter 3 for a fuller description). In order to reduce the computational time 2D-BPM makes certain assumptions. One such assumption is that there is only one vertical mode supported by the cavity and that the mode's horizontal and vertical components are separable. This is a fair assumption for the laser as they are designed to support only the fundamental mode. By using this assumption, one only has to apply full BPM in the horizontal axis in order to simulate the propagation of the many supported modes. However, in the vertical axis one can assume that only one mode is being propagated. Therefore, one can 'compact' the 3D space of the cavity into the 2D space of the horizontal mode by using the well known effective index method. This means that one can simulate the propagation of the light within the laser by only simulating the horizontal component, but by making changes to the effective index it experiences during its propagation. However, as soon as one couples light into the cavity from the outside world it causes problems for our model, as the light may also couple into other vertical modes (analysis reveals that 4 modes can be supported by this device). Due to our previous assumption, however, our model cannot simulate more than one mode in the vertical axis. This problem is reduced by the fact that we know that due to spatial filtering the other modes will decay quickly. Therefore, a modal decomposition of the incident light must be developed to ascertain how much of the incident optical field is coupled into this fundamental mode and how much will be lost. The next section deals with the calculation of how much energy is linked into the fundamental mode.

5.2 The Calculation [16,32-36]

As has been previously stated, the vertical and horizontal modes are separable. Therefore, one can write the electric field components as $\boldsymbol{E}(x,y,z)=\boldsymbol{E}(y)\boldsymbol{E}(x,z)$. This can be seen in figure 5.1, where the vertical and horizontal components have been drawn separately. The maxima of the vertical modal profile under the ridge waveguide region will be in the quantum well. The horizontal model profile is calculated by 2D-BPM *at* this maxima (shown by the horizontal line in figure 5.1).

The laser cavity can support many modes along the horizontal axis and 2D-BPM can handle the propagation of these modes. However, along the vertical axis, 2D-BPM can only propagate in the fundamental mode. Therefore, we need to perform an overlap calculation along the vertical axis to determine how much the vertical mode of the cavity has been excited by the incident radiation. Simply stated we need to know the excited amplitude of the vertical mode in a piece-wise form across the entire horizontal axis of the cavity. To calculate this amplitude, the following mathematics was performed.

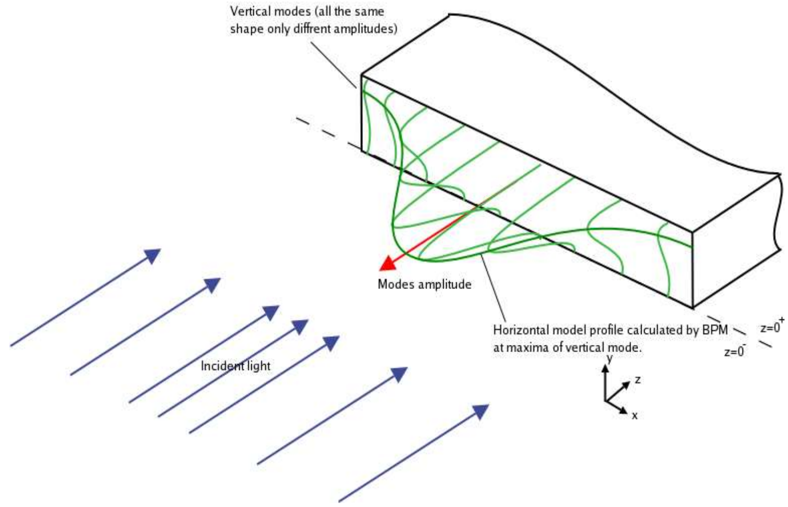

Figure 5.1 The vertical and horizontal mode shapes of the light emitted by the laser. Note this is a very much simplified drawing of the lasers front facet.

In the following pages, the general classical overlap integral for a two dimensional space will be derived. Then we will reexamine it for the vertical mode alone. Following Snyder [37], we can write the general field just within the device ($z=0^{+}$ figure 5.1) as a summation of the propagating modes plus a radiating field (equations 5.1 and 5.2), where $\boldsymbol{E}_n(x,y)$ and $\boldsymbol{H}_n(x,y)$ are the field vectors of the n^{th} propagating mode. C_n is the amplitude of the mode, and $\boldsymbol{E}_r$, $\boldsymbol{H}_r$ are the radiating fields[36].

$$\boldsymbol{E}'(x,y)=\sum_{n=0}^{\infty} C_n \boldsymbol{E}_n(x,y)+\boldsymbol{E}_r(x,y) \tag{5.1}$$

$$\boldsymbol{H}'(x,y)=\sum_{n=0}^{\infty} C_n \boldsymbol{H}_n(x,y)+\boldsymbol{H}_r(x,y) \tag{5.2}$$

If one wishes to examine the contribution of a single mode to the total accepted field with in the device, the constant C_n must be found (where $\boldsymbol{E}_n(x,y)$ is normalized to one). In order to do this we must use orthagonality we begin by multiplying both sides of the equation by $\times \boldsymbol{H}_m(x,y)$.

(5.3)

$$\boldsymbol{E}'(x,y)\times\boldsymbol{H}_m^*(x,y)=\sum_{n=0}^{\infty}C_n\boldsymbol{E}_n(x,y)\times\boldsymbol{H}_m^*(x,y)+\boldsymbol{E}_r\times\boldsymbol{H}_m^*(x,y)$$

Then we integrate over the area of the device. (In practice, one can assume that the integration is done over a large area with periodic boundary conditions.)

$$\iint_{-\infty-\infty}^{\infty\infty}\boldsymbol{E}'(x,y)\times\boldsymbol{H}_m^*(x,y)\,dxdy=\sum_{n=0}^{\infty}\iint_{-\infty-\infty}^{\infty\infty}C_n\boldsymbol{E}_n(x,y)\times\boldsymbol{H}_m^*\,dxdy$$
$$+\iint_{-\infty-\infty}^{\infty\infty}\boldsymbol{E}_r(x,y)\times\boldsymbol{H}_m^*(x,y)\,dxdy \tag{5.4}$$

But we know that

$$0=\iint_{-\infty-\infty}^{\infty\infty}\boldsymbol{E}_n(x,y)\times\boldsymbol{H}_m(x,y)^*\,dxdy=\iint_{-\infty-\infty}^{\infty\infty}\boldsymbol{E}_m(x,y)\times\boldsymbol{H}_n^*(x,y)\,dxdy \tag{5.5}$$

where $n\neq m$ (this also holds for the radiating mode as well). Therefore, we can rewrite 5.4 as

$$\iint_{-\infty-\infty}^{\infty\infty}\boldsymbol{E}'(x,y)\times\boldsymbol{H}_n^*(x,y)\,dxdy=C_n\iint_{-\infty-\infty}^{\infty\infty}\boldsymbol{E}_n(x,y)\times\boldsymbol{H}_n^*(x,y)\,dxdy, \tag{5.6}$$

which can be rearrange to give C_n as

$$C_n=\frac{\iint_{-\infty-\infty}^{\infty\infty}\boldsymbol{E}'(x,y)\times\boldsymbol{H}_n^*(x,y)\,dxdy}{\iint_{-\infty-\infty}^{\infty\infty}\boldsymbol{E}_n(x,y)\times\boldsymbol{H}_n^*(x,y)\,dxdy} \tag{5.7}$$

Now we shall take a short detour to produce the classical overlap integral expression for power coupled into the device. We start by considering the total power coupled into the mode by integrating the Pointing vector over the modal cross section.

$$P_n=C_n^2\iint_{-\infty-\infty}^{\infty\infty}\boldsymbol{E}_{\mathrm{n}}(x,y)\times\boldsymbol{H}_n^*(x,y)\,dxdy \tag{5.8}$$

Substituting in C_n as found previously we get

$$P_n=\frac{\iint_{-\infty-\infty}^{\infty\infty}\boldsymbol{E}_{\mathrm{n}}(x,y)\times\boldsymbol{H}_n^*(x,y)\,dxdy\left(\iint_{-\infty-\infty}^{\infty\infty}\boldsymbol{E}'(x,y)\times\boldsymbol{H}_n^*(x,y)\,dxdy\right)^2}{\left(\iint_{-\infty-\infty}^{\infty\infty}\boldsymbol{E}_n(x,y)\times\boldsymbol{H}_n^*(x,y)\,dxdy\right)^2} \tag{5.9}$$

and dividing by the total incident power,

$$P_{total}=\int_{-\infty}^{\infty}\int_{-\infty}^{\infty} \boldsymbol{E}^{'}(x,y)\times\boldsymbol{H}^{'*}(x,y)\,dxdy,$$

we get the classic expression for the coupling efficiency as described by Neumann[32].

$$\eta=\frac{P_n}{P_{total}}=\frac{\left(\int_{-\infty}^{\infty}\int_{-\infty}^{\infty} \boldsymbol{E}^{'}(x,y)\times\boldsymbol{H}_n^{*}(x,y)\,dxdy\right)^2}{\int_{-\infty}^{\infty}\int_{-\infty}^{\infty} \boldsymbol{E}_n(x,y)\times\boldsymbol{H}_n^{*}(x,y)\,dxdy\int_{-\infty}^{\infty}\int_{-\infty}^{\infty} \boldsymbol{E}^{'}(x,y)\times\boldsymbol{H}^{'*}(x,y)\,dxdy}$$

(5.10)

However a very large number of modes can be supported by the device in the horizontal axis so the overlap integral only needs to be performed in the vertical axis, therefore 5.1,5,2 can be rewritten for the vertical modes alone producing a piece wise value for C_n along the horizontal (X) axis.

$$\boldsymbol{E}^{'}(y)=\sum_{n=0}^{\infty} C_n(X)\,\boldsymbol{E}_n(y)+\boldsymbol{E}_r(y)$$

(5.11)

$$\boldsymbol{H}^{'}(y)=\sum_{n=0}^{\infty} C_n(X)\,\boldsymbol{H}_n(y)+\boldsymbol{H}_r(y)$$

(5.12)

We can rewrite 5.11 as

$$\int_{-\infty}^{\infty} \boldsymbol{E}^{'}(y)\times\boldsymbol{H}_m^{*}(y)\,dy=\sum_{n=0}^{\infty}\int_{-\infty}^{\infty} C_n(X)\,\boldsymbol{E}_n(y)\times\boldsymbol{H}_m^{*}(y)\,dy+\int_{-\infty}^{\infty}\boldsymbol{E}_r(y)\times\boldsymbol{H}_m^{*}(y)\,dy$$

(5.13)

Using orthagonality we can again say,

$$0=\int_{-\infty}^{\infty} \boldsymbol{E}_n(y)\times\boldsymbol{H}_m(y)^{*}\,dy=\int_{-\infty}^{\infty} \boldsymbol{E}_m(y)\times\boldsymbol{H}_n^{*}(y)\,dy,$$

(5.14)

if $n\neq m$. Thus, equation 5.13 can be written and rearranged as

$$C_n(X)=\frac{\int_{-\infty}^{\infty} \boldsymbol{E}^{'}(y)\times\boldsymbol{H}_n^{*}(y)\,dy}{\int_{-\infty}^{\infty} \boldsymbol{E}_n(y)\times\boldsymbol{H}_n^{*}(y)\,dy},$$

(5.15)

Which for TE waves can be simplified to

(5.16)

$$C_n(X) = \frac{\int_{-\infty}^{\infty} \boldsymbol{E}'(y) \cdot \boldsymbol{E}_n^*(y)\,dy}{\int_{-\infty}^{\infty} \boldsymbol{E}_n(y) \cdot \boldsymbol{E}_n^*(y)\,dy},$$

As TE are being used we can assume that the electric field is tangential to the boundary of the device, therefore the boundary condition, $\boldsymbol{E}_{1\tan}(y) = \boldsymbol{E}_{2\tan}(y)$, holds. So no adjustment of the electric field is needed when moving between $z=0^+$ and $z=0^-$. The remaining step is to rewrite equation 5.16 in a sampled for that can be used on discreet data.

$$C_n(X) = \frac{\sum_{-\infty}^{\infty} \boldsymbol{E}'(y) \cdot \boldsymbol{E}_n^*(y)\,dy}{\sum_{-\infty}^{\infty} \boldsymbol{E}_n(y) \cdot \boldsymbol{E}_n^*(y)\,dy}, \tag{5.18}$$

$C_n(X)$ will then be the amplitude of the excited mode at position X across the facet. Equation 5.19 was then included in to the LabVIEW optical simulation software as a vi.

5.3 Implementation of the overlap integral as a LabView vi

It was decided to incorporate the overlap integral into its own vi, so that it could be re-used in other pieces of code and programs if later required. A screen shot of the vi is shown below in figure 5.2.

Figure 5.2 A screen shot of the vi which implements the overlap integral.

Conan calculates the normalized mode shape of the vertical fundamental mode of the device. This is read in and placed on the input of the vi labeled "Input mode of the light". The vi then accepts a complex 2D array representing the incident light upon the front facet. Equation 5.19 is applied piece-wise across the facet and a 1D array is generated, which represents the amplitude of the excited vertical modes.

6. The bidirectional interface

An overview of the bidirectional software interface written in Labview

6.1 Background

The bidirectional interface was originally intended to form a bridge between Conan and a third party optical package. Its purpose was to convert file formats, perform any mathematics needed (i.e. the overlap integral or normalization) and control the execution of both the laser simulator and optical simulator. It was intended to use this interface to synchronize one simulator with the other, so that as one simulator finished one iteration sequence, the results were passed to the other simulator in this way the entire laser-opto system could be solved without the need to write a new simulator. The programing language chosen for this task was LabVIEW mainly because of its ability to produce easy to use graphical interfaces, combined with the fact that it has many builtin functions for data processing .

6.2 An overview of the execution cycle of the bidirectional interface

The execution cycle is shown below in figure 6.1. The first thing one notices about the execution of the program is that it is a loop. It just shuffles data back and forth between the simulators until convergence occurs. The first step for the bidirectional interface is to execute Conan (1. in figure 6.1). The interface then goes into a loop checking every 500ms for a file called 'go' to be generated within Conans home directory (2). Once this file has been generated, the bidirectional interface knows that Conan has finished one full sweep of the cavity (section 3.2) and is now waiting for the back reflected light to be returned to it. The interface then reads in the files containing the near field of the laser and converts them in to a format readable by the optical simulator (3). Then using a windows API call, it executes the optical simulator (4a). LabVIEW then waits for the windows to finish with the execution of the optical simulator (4b). The overlap integral is then performed and the data is converted to the output format Conan can read.(5). This data is then saved to disk ready for Conan to resume its execution.(5) Conan is then unpaused by removing the file 'go'(6).

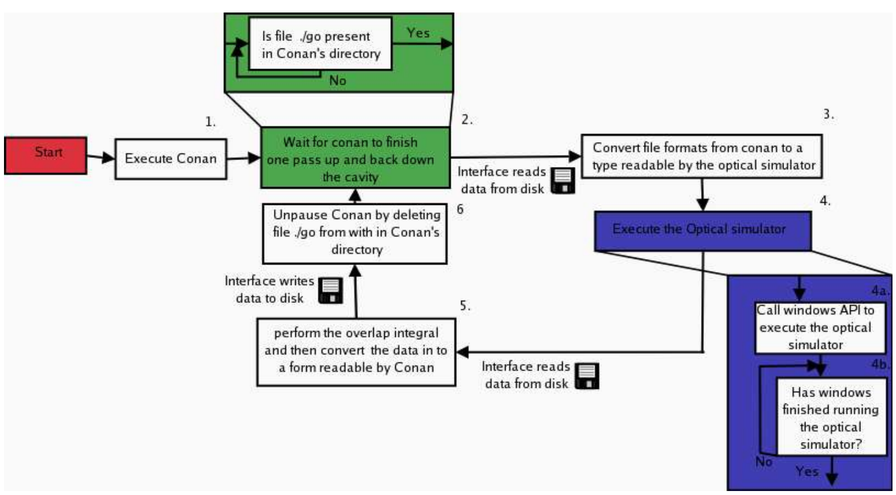

Figure 6.1 The execution cycle of the bidirectional interface.

Conan notices that this file is missing and that it should read in the updated backreflected field and to continue its solution of the laser cavity. This process continues until conversion has occurred.

Section 6.1-2 was a general overview of operation of the bidirectional interface. The next section will examine each step in somewhat more detail, describing the operation of some of the more important vi's.

6.3 Execute Conan (1)

This is the first stage in the simulation cycle. LabVIEW has a built-in vi, which will tell windows to execute a program and not wait for its completion before resuming the execution of the LabVIEW program. This was used, it only needed to be provided with the path of Conan.

6.4 Wait for Conan to finish one iteration (2)

In section 3.2, it was described that when Conan has finished one iteration, it writes out the near field to disk. Then generates a file called 'go' which it waits to be deleted before rereading the near field back from disk and continuing its solution of the device equations. The LabVIEW program, on the other hand, waits for the file 'go' to appear, which is an indication that Conan has finished one iteration and it is time to start processing the data that Conan has written to disk. The version of LabVIEW used possesses no function to wait for a file to be generated. Therefore, one had to be made. It is shown below in figure 6.2. The path of the file to wait for is passed on to 'Lock file' and the other input entitled 'Type of lock' sets if the vi is to wait for a file to be deleted (false) or generated (true).

The Lock vi generated to wait for a file figure 6.2

6.5 Convert the file formats into a type readable by the optical simulator (3)

As Conan assumes the separability of the solution, when it writes data to disk it is convenient to write the horizontal mode profile and vertical mode profile in sperate files as 1D arrays. However, the optical simulator expects data to be given to it in a complex 2D array. This means that Conan's output files must be read in by the interface and 'multiplied' together to form the 2D field. A vi was written to do this and is shown in figure 6.3. The path of the vertical mode is placed on 'Path of field1D.txt (V) mode'. The path of the file containing the horizontal mode is placed on 'path of field1.txt (H) mode'. The output is placed on '2D generated output array' and the other control lines are used for debugging.

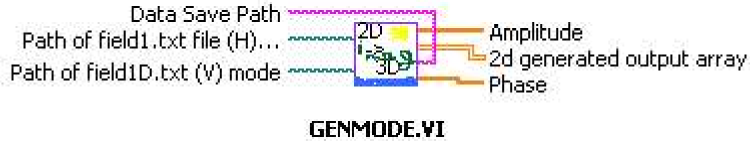

The Genmode vi Figure 6.3

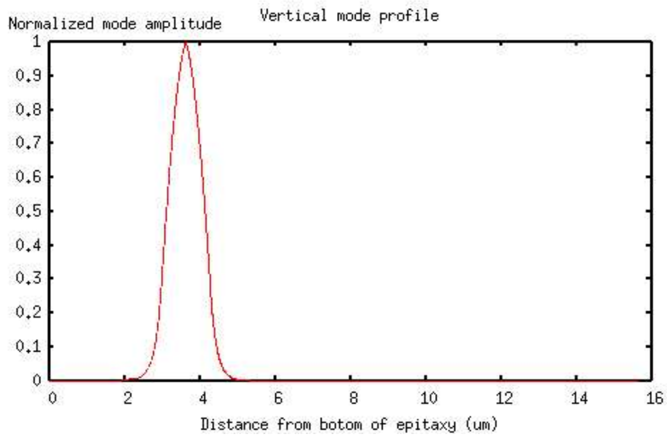

Figure 6.4, The vertical mode profile.

The discussion of this vi brings us to another important point. Conan's vertical mode contains far more data points/m than Conan's horizontal mode. The horizontal mode consists of about 250 data points and the vertical mode profile given in field1D.txt contains over 5000 entries and most of these data points are no where near the quantum well region and never emit light (and were therefore were zero - a plot of field1D.txt is shown in figure 6.4). About one sixth of the field1D.txt contains no data (figure 6.4). It made no sense to use the entirety of this file as the vertical mode, as most of it was empty. Only the peak shown in figure 6.4 contains information about the mode profile. Therefore a function had to be written to firstly cut this mode out of the data file. Thereby saving memory and then to sample the vertical mode so that it was sampled at a comparable rate to the horizontal mode. Thus 5000 data points were brought down to 50. This vi is shown below in figure 6.5, an array containing field1D.txt is placed on 'Input array from field1.txt'. The number of points to be returned placed on 'Number of vertical output points' and the output array is returned in 'Output'. This saving of memory may not seem very worth while, but when one considers that most diffraction will occur in the fast axis, and the further one propagates the light the more it will diffract and the more it diffracts the more memory will be required for the simulation. Cutting down the resolution of the vertical mode to a more sensible figure can make the difference between a simulation requiring giga bytes of memory to run and only a few tens of megabytes.

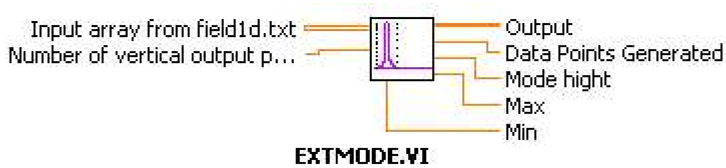

Figure 6.5 The extract mode vi

Before this vi, or indeed any other vi can be used, some data has to be read from an input file. There are various problems associated with getting LabVIEW to read poorly formatted files (Conan has many of these). Examples of a poorly formatted files are ones in which text has mixed in with numbers, and files which separate the column with different characters, for example comas or spaces will cause problems for LabVIEW. When one does not pay attention to this, LabVIEW can easily get confused when reading in a file and think it is reading in a different line to the one it is actuallyreading. This problem was solved in a two step process. Firstly, a function was written to take in a string containing numbers formatted in a disorganized fashion and convert them into an array of numbers. An example of the operation would be to take in a string such as “1,2,3, 4,5 8 9 10 1.2e-12 4 –data point 7--” and convert the number in to a clean array of numbers such as in table 6.1

Array Element	0	1	2	3	4	5	6	7	8	9
Value Decoded	1	2	3	4	5	8	10	1.2e-12	4	7

The output of extnum.vi Table 6.1

The algorithm acts as a filter function only letting through numbers, full stops, comas, minuses and the letter e. Such a filter function was written and incorporated in to a vi called Extnum.vi (Extract number). It contains an input which is the string of data to be operated upon. The output is a clean array of numbers and an integer number holding the number of elements in the array. If no numbers were found in the array, the wire 'No Match' returns -1. This vi is shown below in figure 6.6

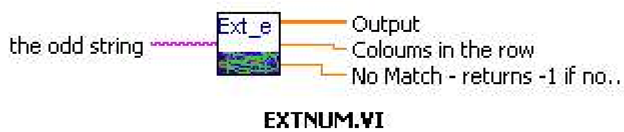

Fig 6.6 Extract Number.vi

Once this function was written, it was then incorporated in to a vi called Dattoarry.vi (Data to array.vi, see figure 6.7).

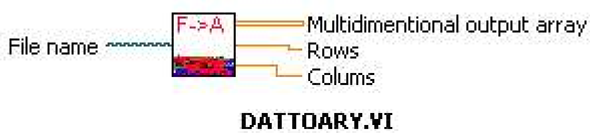

Figure 6.7

This vi accepts a file name, opens the file, reads in a line, applies the extract number.vi to the line. Then it reads in the next line, applies the extract number.vi again and repeats this process until the entire file has been read. The result is an array containing the table, which was in the text file. This vi has been used over and over again, and simplifies the process of reading in a file. A vi which writes any array to a file was also written for completeness. This is shown below in figure 6.8

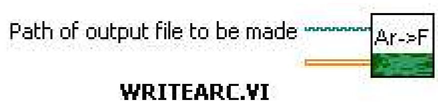

Figure 6.8 Write an array to a file.vi

The above vis are coupled together to generate the file type the optical simulator requires. It was well worth while writing solid functions to solve these simple problems such as reliably reading in and easily writing out files and sped up the development time. At the beginning of the development of the interface, many problems were encountered with Conans files having text or odd characters inserted in the middle of them. By writing these vis carefully, these problems were never reencountered.

6.6 Execution of the optical simulator (4)

At the moment the interface communicates with a custom optical simulator for which we have the source code. However, in the future it may be desired to couple the interface to a second party simulator, for which we may not have the source code. Therefore, it was decided not to use the 'lock' files as a communication channel between the optical simulator and the interface (as was done for Conan), because any second party optical simulator will certainly not be designed to generate any of these files. This meant that we had to have a way of knowing when the optical simulator had finished its simulation. Unfortunately, the version of LabVIEW used provides no function to wait for a program to finish executing. Therefore a windows dynamic library (dll) file was written to act as an interface between some of the more advanced windows API calls and LabVIEW. A wrapper vi was then written to call and interface this dll. The wrapper vi first creates a file called 'lock' in the same directory as the program which has been called. For example, it was desired to execute Conan.exe in directory c:\conan. A file called c:\conan\lock is generated and then the vi executes the dll. This dll calls the windows API call system_execA , which always halts the execution of the current program until the new program has finished execution. When the desired program has finished running, windows continues to execute the dll, which next deletes the lock file and exits itself. Meanwhile, the LabVIEW program has been waiting for the the lock file to be deleted. When the lock file is deleted, LabVIEW then knows that the program which was requested to be run, is in fact finished LabVIEW can read back in the data from the optical simulator.

Fig 6.9 The Runner VI

The vi itself is shown above in figure 6.9. It was mentioned in Chapter 5 that the optical simulator has a configuration file which hands certain device perimeters to it. Conan also has a set of configuration files which contain the same information. Therefore, it made sense to update the optical simulator's configuration files from Conan's configuration files every time the optical simulator was run, so that there would never be any mismatch. Of course, the simplest solution would be to get the optical simulator reading Conan's configuration files, but again, a second party optical simulator would not be able to do this. So, a few vis were written to interface with Conans dbt.txt file (one of its major configuration files) to extract critical information. Figure 6.10 shows the vi which gets the width of the taper.

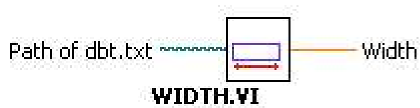

Figure 6.10 Width.vi,this returns the width of the taper

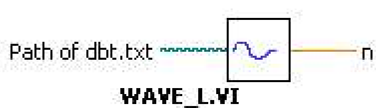

Figure 6.11 Get wave length.vi, the vi which gets the simulated wave length from Conans configuration files.

These values are then compiled together to update the configuration file Config.txt used by the optical simulator.

6.7 Perform the overlap integral – do post processing for the optical simulator (5)

Once the optical interface has registered that the optical simulator is finished, it reads in the complex 2D field from the optical simulator's output file. The overlap integral is performed as described in chapter 5 (specifically section 5.3.) The post processing for the optical components is then performed, as described in section 4.9 onwards. The optical post processing will involve a change of phase for the light by 180^{o} . The laser's front facet reflectivity will be taken in to account as well as the lenses reflectivity, (again see section 5.3). The reflectivity of the front facet is retrieved from Conans configuration files with the Get reflectivity vi. This is shown below in figure 6.12.

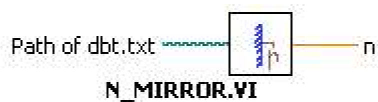

Figure 6.12 The Get reflectivity vi

The path of dbt.txt (the file containing the reflectivity of the front facet) is placed on one input of the vi and the reflectivity is returned on the yellow wire.

6.8 Run Conan again (6)

Once the new field at the front facet has been written to disk in a form Conan can read (1D complex array), everything is ready for Conan to be restarted. It has, in the meantime, been patently waiting in memory ready to be reactivated. The file 'go' is deleted with LabVIEWS's delete command. Conan will then read in the new near field from disk, updates its electric field array and continues to solve the device equations until one more iteration has been completed. The Labview program then returns to stage 2 and waits for the file 'go' to be regenerated before starting the cycle again.

6.9 The user interface

The user interface was designed not to be too complex. After all this was only meant to be an interface between the optical simulator and Conan and only needed to show information relating to the simulation. It was designed to display the height of the output mode of light, the width of taper, iteration number , number of times to iterated, wave length and mirror reflectivity. This information was designed to be just a check on the simulation state. There were two controls to control the progression of the simulation. One could either click the button 'iterate until convergence' on, so that the simulation would iterate until convergence. Alternatively one could select a number of iterations to perform by typing in the wanted number of iterations into the iteration number box. All these input controls and out put fields are shown as they appear in the LabVIEW application shown in figure 6.13.

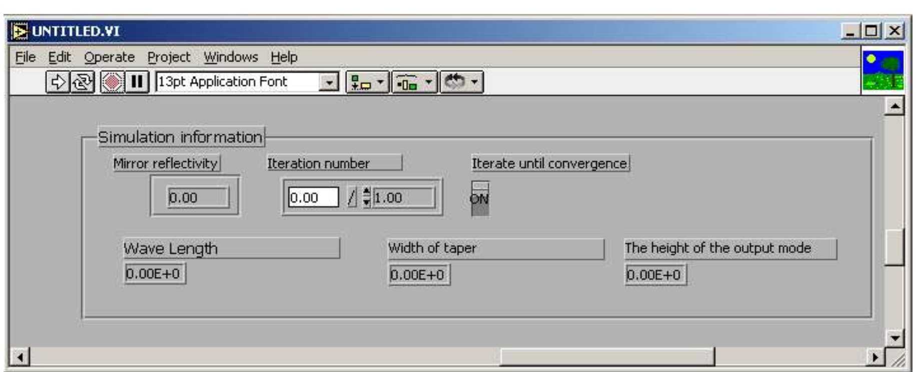

The interface has another set of inputs. These inputs tell the simulator where Conan is located, where the optical simulator is located and where any other critical files are located. This is shown below in figure 6.14.

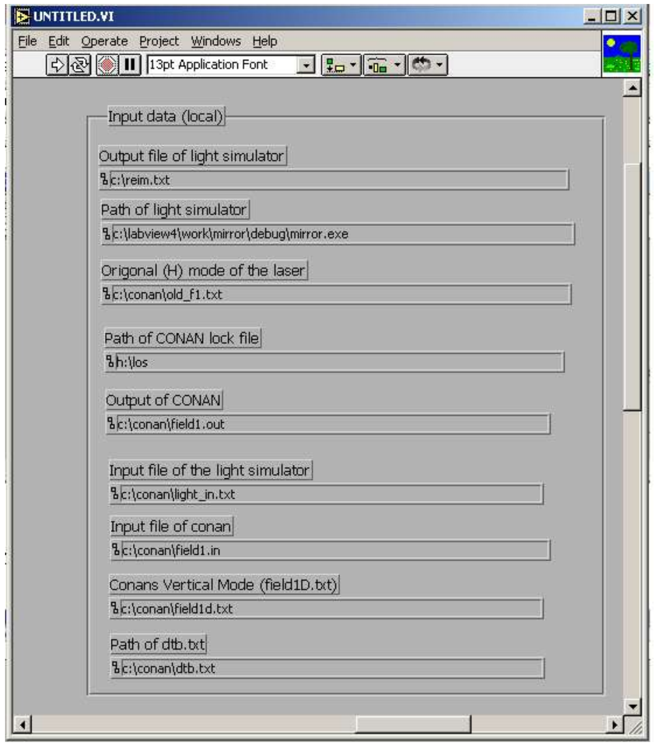

Figure 6.14 The interfaces configuration boxes.

Graphs were added to the application to monitor the simulation as it progressed. The phase and the amplitude of the light from the laser can be examined, as well as the light incident upon the facet, the light linked into the fundamental vertical mode of the laser, and the addition of the back coupled light with that light reflected off the front facet. An example of a typical simulation running is shown below in figure 6.15.

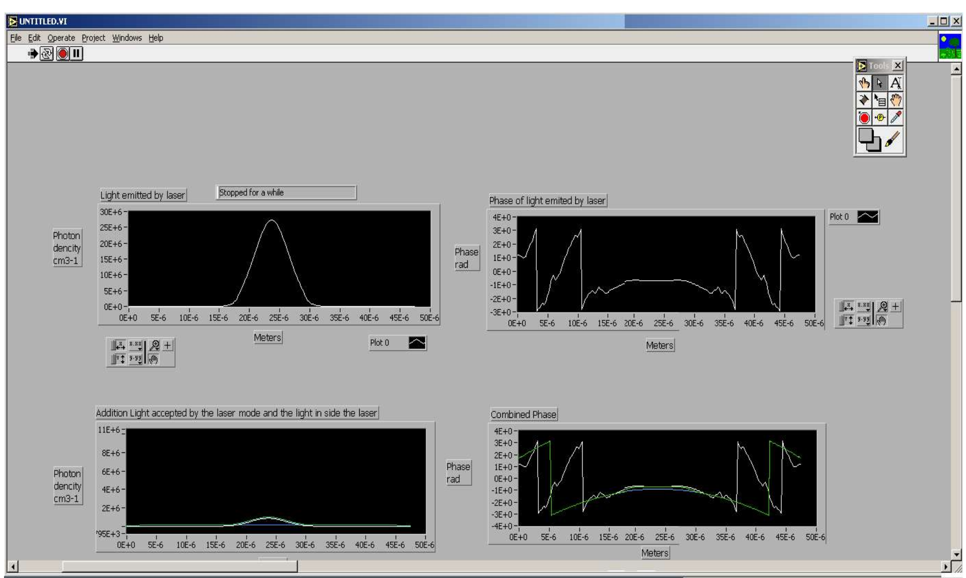

Figure 6.15 An example of a typical running simulation.

At every stage of the simulation, the results were saved to disk. This was to check for errors in the program and to make sure that no data would be lost, so that no experiment would have to be re-run. To do this, a special vi was written, which could be given a complex array consisting of a real part and an imaginary part. Shown in figure 6.16, it saves two files - one called filename.exponent and the other called filename.argument. Theses files contain the exponent and the argument of the data passed to it in a complex array. This function was very useful for saving the phase/amplitude information during the simulations.

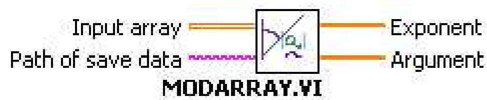

Figure 6.16 The Mod array vi, used to save the phase
and the field profile in different files ready to be plotted.

6.10 A small compiler setback

A small problem arose after about two months in to the project. By this stage, the LabView interface had been developed on a PC and the modifications to Conan were in the process of being tested on a UNIX box. The next step was to recompile the FORTRAN 90 code of Conan on the PC and get LabVIEW working together with Conan. Unfortunately, Conan was originally written on Digital FORTRAN (formally Microsoft F90) in Madrid and a version of FORTRAN which comes with Digital UNIX in Nottingham. It compiled well on these compilers. Unfortunately, the University had since adopted Salford FORTRAN, which has compatibility issues with Digital FORTRAN. Whilst a new copy of FORTRAN was ordered, it was decided that instead of halting development, it was best to press on as time was limited. So a copy of samba (www.samba.org) was installed on the UNIX box. Samba is a free program released under the GNU license used for sharing files between UNIX file serves and windows clients. This software allowed Conan on the UNIX box and LabVIEW and the optical simulator running on the PC to swap files. This enabled the project work to continue until a copy of FORTRAN for a PC was made available.

7. Experimental Procedure

An overview of the experiments performed

7.1 Running the simulation

As soon as the simulator had been completed the experimental phase of the project started. It took about 12.5hours for an experiment to run to convergence, this meant that one experiment could be run per day, or five experiments per week. As mentioned when discussing the selection of the laser device, nobody has reported attempting such experiments before. This made it difficult to select which paramaters to vary in the experiment. Therefore, it was very much a case of performing one experiment then examining the results before deciding on the direction the next experiment should take. However, before any experimental tests were run with the optical simulator, it was important to establish how well the laser performed without any optics in front of it. Therefore the optical interface to Conan was disabled and Conan was allowed to simulate the laser alone. Every time a simulation was performed with a slightly different device structure, Conan was run alone for one simulation, to get a result to which later results (with optics) could be compared. After re-enabling the optical interface, the first experiment was performed with a piece of flat BK7 Glass placed directly in front of the laser at a distance of 250λ . A piece of flat BK7 glass was chosen for the first set of experiments because it was simple to simulate and the results would be easy to understand. More complex structures could be simulated later without much more effort, but it is better to start off with a simple system and increase its complexity rather than working the other way around. The distance may seem relatively short, but is not unrealistic. When one considers the large amount of diffraction in the fast axis, one usually needs to place a lens very close to the laser to correct this. Secondly, when one considers the relatively new field of optical interconnects[41-43], there is often not room for much distance between the lens and the laser. In practice, lenses are sometimes placed directly on top of lasers. Another good reason for choosing this short distance was that a rough calculation showed that at least 1% of the back traveling light within the tapered region of the cavity would be due to the external optics, therefore a noticeable effect on the laser was expected. This distance could be increased in later experiments.

When one considers that any light propagating backwards within the laser will be a summation of the light reflected from the internal mirror and the light reflected back off the internal optics, it becomes clear that the two waves could positively and destructively interfere. This interference is a function of phase and thus of total distance propagated. Therefore, it made sense to repeat the experiment for different propagation distances separated by only one quarter of a wavelength. This was done, the experiments performed are shown in table 7.1. Note this table shows *total propagation distance* i.e. *twice* the distance to the external optics.

Experiment	***Front Facet reflectivity***	***Total propagation distance***
1	3%	500.00λ
2	3%	500.25λ
3	3%	500.50λ

Experiment	*Front Facet reflectivity*	*Total propagation distance*
4	3%	500.75 λ
5	3%	501.00 λ

Table 7.1 The first set of experiments performed

It is well known that tapered lasers with very low front face reflectivities (0.1%) are less likely to suffer from effects such as spatial hole burning because the back reflections from the tapered amplifier are weaker so do not seed these effects in the master oscillator. However, with a front facet power reflectivity 10-30 times less than a conventional high power laser they could be more susceptible to feedback from the outside world. For example there is less back-reflected light from the internal mirror, so that the back-reflected light from the optics will account for a greater proportion of the back traveling radiation. Thus a small change in the external optics due to heat expansion of the system may lead to a large change in the beam properties. Secondly more light can pass through the front facet from the outside world into the laser due to its lower reflectivity, so not only will more light be allowed into the laser form the outside world, but the light which is allowed in to the laser will be larger in proportion to the light reflected from the internal mirror. The following experiments shown in table 7.2 were also performed.

Experiment	*Front Facet reflectivity*	*Total propagation distance*
1	0.1%	500.00 λ
2	0.1%	500.25 λ
3	0.1%	500.50 λ
4	0.1%	500.75 λ
5	0.1%	501.00 λ

Table 7.2 The second set of experiments performed

Because the front facet reflectivity was so much lower, another set of experiments was performed at double the distance, as shown in table 7.3

Experiment	*Front Facet reflectivity*	*Total propagation distance*
1	0.1%	1000.00 λ
2	0.1%	1000.25 λ
3	0.1%	1000.50 λ
4	0.1%	1000.75 λ
5	0.1%	1001.00 λ

Table 7.3 The third set of experiments performed.

8. Results and Analysis of results

8.1 A front facet reflectivity of 3%, with the light propagated a distance of 500-501 wavelengths

In a real experiment, the light makes a round trip from the front of the laser to the flat piece of glass and back again. This also happens in the simulated experiment, but we have the added advantage of being able to easily examine the amplitude and phase of the light at each stage of this process. The first step is as the light leaves the laser's facet as shown in figure 8.1a (amplitude of the optical electric field in the near field of the laser). Figure 8.1a, as with all the figures in this chapter, is of the converged solution. Thus, although we may be talking about the light leaving the facet, it is not the first step in the iterative process and one can assume that the system has in fact stabilized. It was thought that as one varied the distance of the external optics by fractions of a wavelength, constructive and destructive interference of the back propagated light with the light within the laser's cavity may be observed. The first thing one notices about figure 8.1a is that varying the distance to the mirror has almost no impact on the amplitude of the near field. If one examines figure 8.1b, which shows the phase across the taper plotted for all the experiments run, one can see that the phase of the light emitted by the laser has indeed been altered by the back reflections off the external optics. The key feature to this graph is that in the central region of the taper where the electric field is strongest, there is a relatively small change in the value of phase when compared to the simulation of the laser run without any external optics (the brown line). However, as one examines the regions of the taper outside the main beam, a large alteration in phase can be seen. This shows that the back-coupled light is having an effect on the laser. However, in the main beam region of the taper, it has only a tiny effect because very little light is back coupled. Outside the main beam the effect is greater because the relative magnitude of the back coupled light compared to the light being emitted by the laser is larger. So it has been established that the back reflected light does in fact have an impact on light emitted by the laser. Now, if one goes back and re-examines the peak of the curve in figure 8.1a, a very slight trace of color can be seen. The peak of 8.1a has been expanded in figure 8.1c

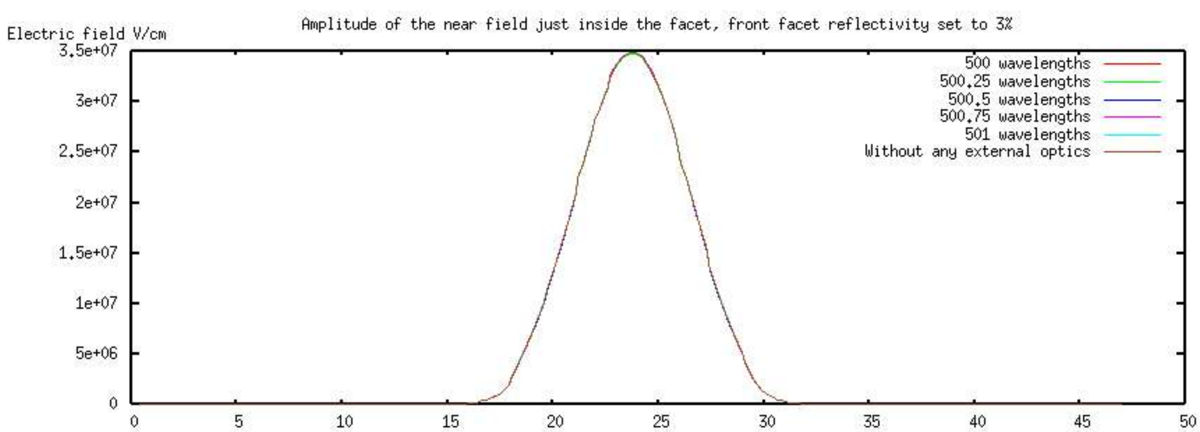

Figure 8.1a The amplitude of the electric field just inside the facet.

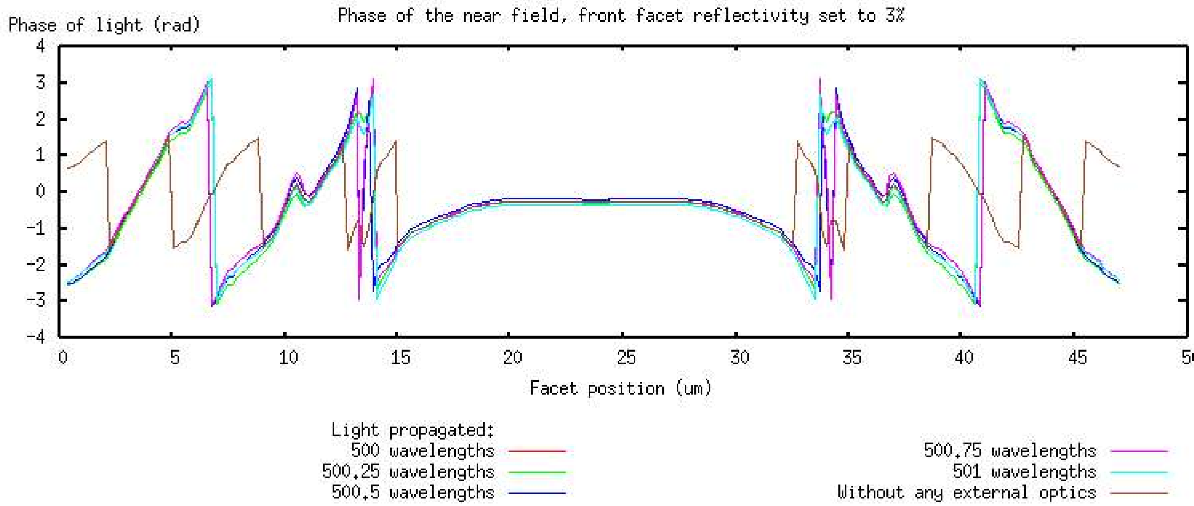

Figure 8.1b The phase of the near field inside the facet.

This shows that there is a very slight variation in amplitude of the main beam as the optics are moved. This can be related to constructive and destructive interference by examining the phase of the back reflected light from the external optics (figure 8.1d) and the phase of the light reflected off the internal mirror figure 8.1f. These graphs are relatively complex, so it is worth explaining them a bit before we go any further. The bottom axis and left hand scale refer to the phase plotted across the entirety of the taper. The top x axis and the right hand y axis refer to a plot of the phase from the 19-29 μm section of the taper. This has been done because the majority of the light is emitted in the 19-29 μm region. The data from the 19-29 μm region is indicated by the words "zoomed in" in the key.

In figure 8.1c the simulated system with the greatest amplitude of emitted light is the one represented by the purple line (500.75 wavelengths). If one now examines the phase difference between the back reflected light from the internal mirror and the optics, it can be seen that there is a difference of about 0.25rad in the center of the beam. Thus, they are interfering constructively. If one now finds the system with the lowest level of emitted light in figure 8.1c and examines the phase difference once again for this system's back reflected light, there is a phase difference of $\sim 1.05\pi rad$ in the center of the beam. Thus the fields are 180^{o} out of phase and constructive interference is occurring. This process can be repeated for the other systems, and it will be seen that the more in phase the back reflected light from the front facet and the external optics are, the larger the amplitude of the near field will be. The phase of the *total* back reflected light within the laser traveling back down the fact has been plotted in figure 8.1f for completeness. It can be said from this observation that the back reflected light has the ability to affect the amplitude of the laser's emitted light by a small amount and it is due to constructive interference. However, what is more interesting is that it also has the ability to improve the mode shape of the emitted light. If one once again examines figures 8.1d, the phase of the back reflected light from the optics between 19-29um is effectively constant. However if one examines the back reflected light from the front facet, it starts to drop off, this means that for the systems whose light was perfectly constructively interfering in the center of the beam, will, at the edges of the beam not interfere so constructively and in an extreme case interfere destructively. This can be seen by examining the phase in figures 8.1d-e. The net result will be that the height of the mode in the center of the beam will be increased and that the height of the mode at the edge of the beam will be decreased. Thus, the mode will narrow (improve in quality). The opposite is true for a system whose light is perfectly destructively interfering at the beams center, the light on the outside of the beam will interfere less destructively or in the extreme case constructively. In this experiment there is very little light accepted into the laser due to the high reflectivity of the front facet, therefore this effect can hardly be seen, however in later experiments it becomes more pronounced. Figure 8.1g demonstrates how how little light is accepted into the laser's cavity from the outside world, in comparison to the back reflected light off the lasers front facet, the combination of the light coming from the outside world and that reflected back off the front facet have also been plotted in this graph taking into account phase.

In the next section, the reflectivity of the front facet will be lowered, this will have two effects, firstly it will allow more light in from the outside world, but also it will decrease the amount of back reflected light from the front facet, thus the back reflected light off the external optics will account for a far larger proportion of the light traveling back down the cavity to the master oscillator.

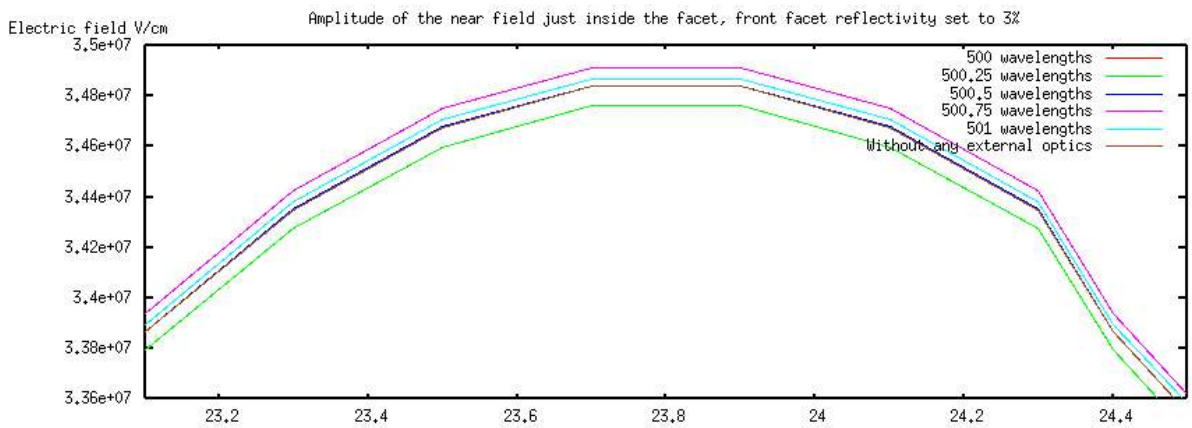

Figure 8.1c The amplitude of the electric field just in side the facet between 23.1um and 24.5um across the facet.

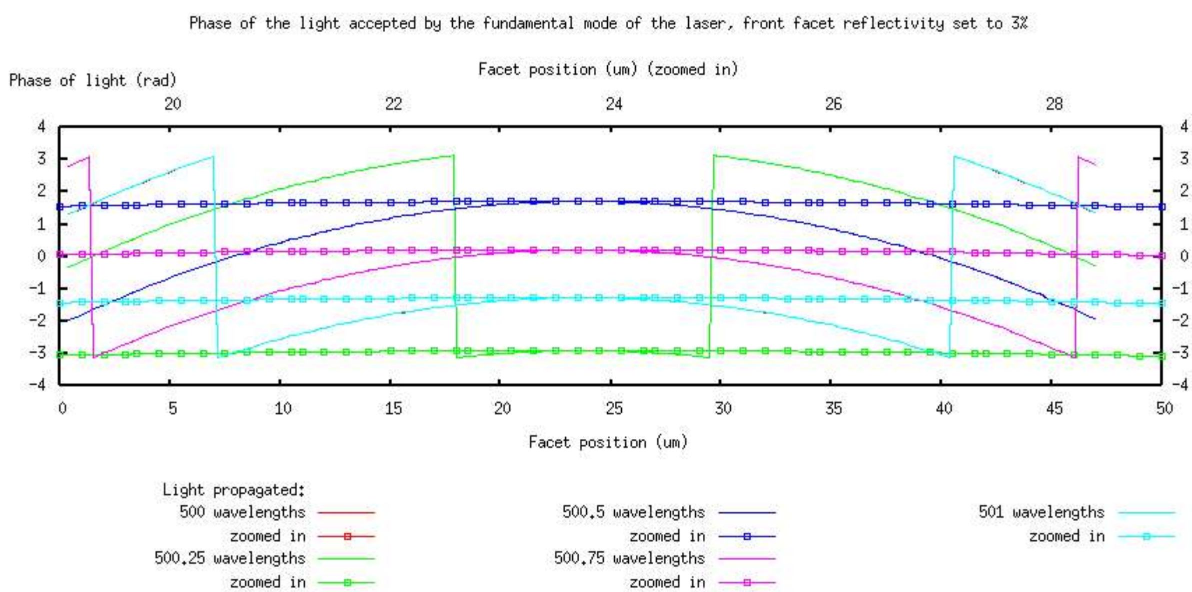

Figure 8.1d Phase of the light coupled back into the fundamental mode of the laser.

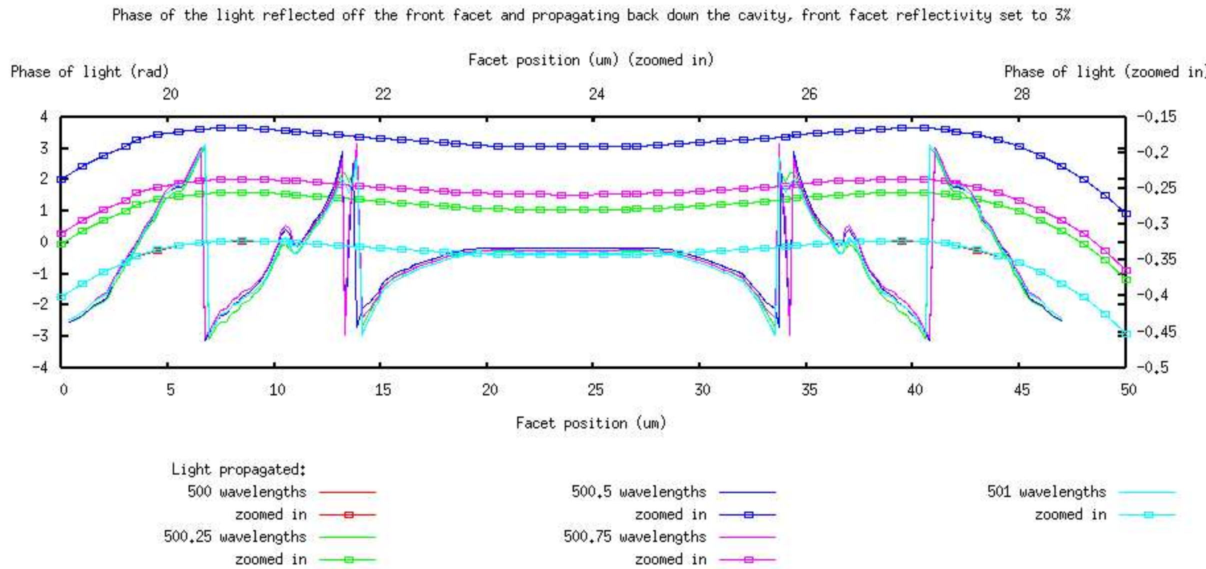

Figure 8.1e Amplitude of light reflected back off the internal mirror traveling back down the cavity.

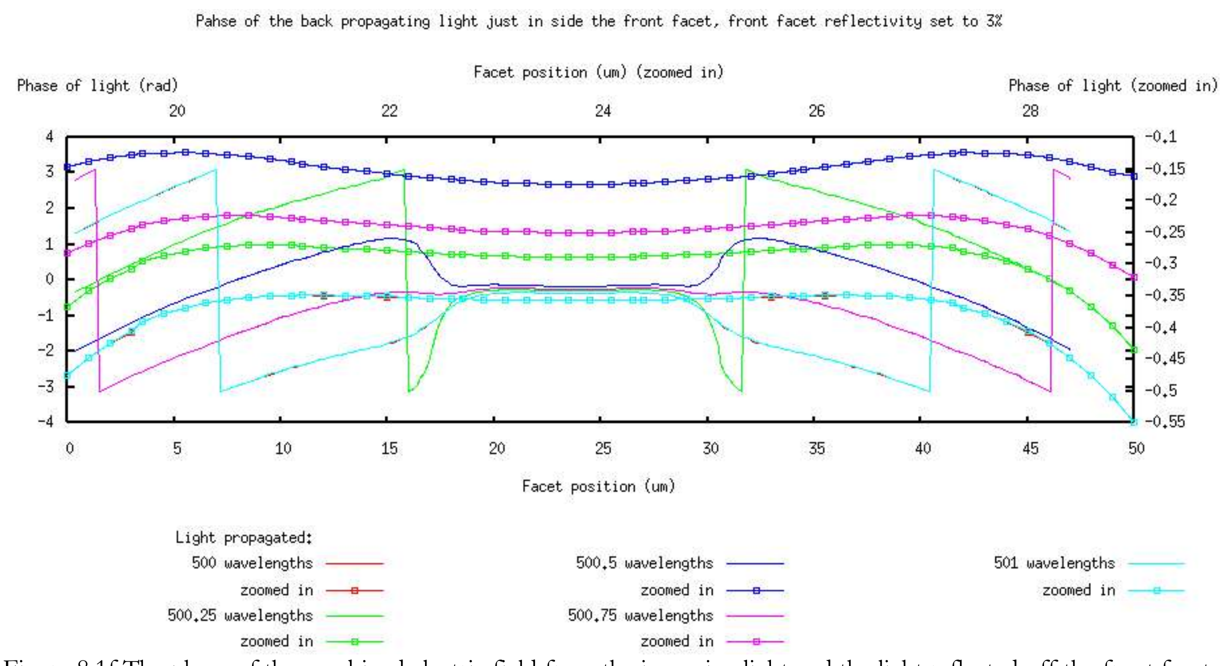

Figure 8.1f The phase of the combined electric field from the incoming light and the light reflected off the front facet of the laser.

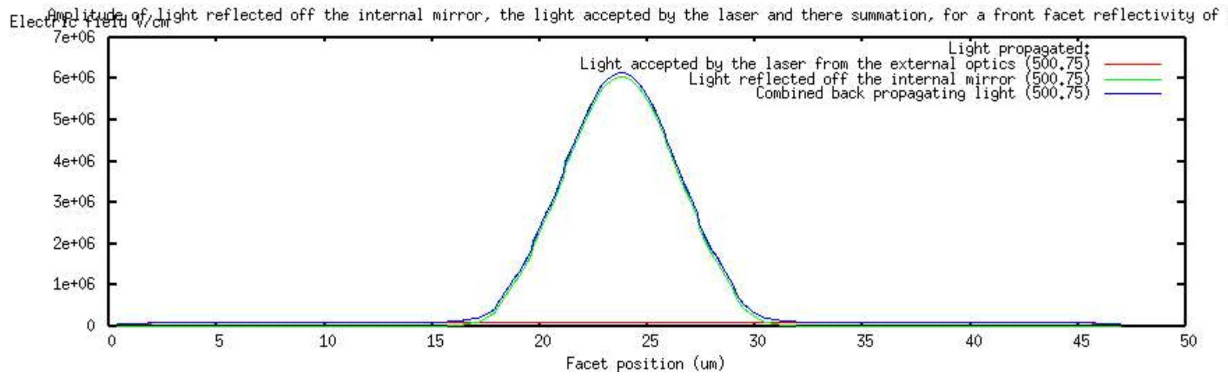

Figure 8.1g A plot of the electric field accepted by the laser from the external optics, the electric field reflected off the internal mirror and the combination of these two taking in to account the difference in phase. The noticeable thing about this graph is how very little field is accepted into the laser from the external optics compared to how much is reflected off the internal mirror.

8.2 A front facet reflectivity 0.1% with the light propagated a distance of 500 wavelengths

As soon as one compares figure 8.2a and figure 8.1a, without any further analysis it can be instantly seen that by lowering the reflectivity of the front facet the back reflected light starts to have a much more pronounced effect on the laser's beam. Amplitude fluctuations of 4% are seen. One can again relate the effects to destructive and constructive interference by examining the phase of the back reflected light of the external optics and light reflected back off the front facet. The peak of the curve in figure 8.2a has been expanded and is presented in figure 8.2b

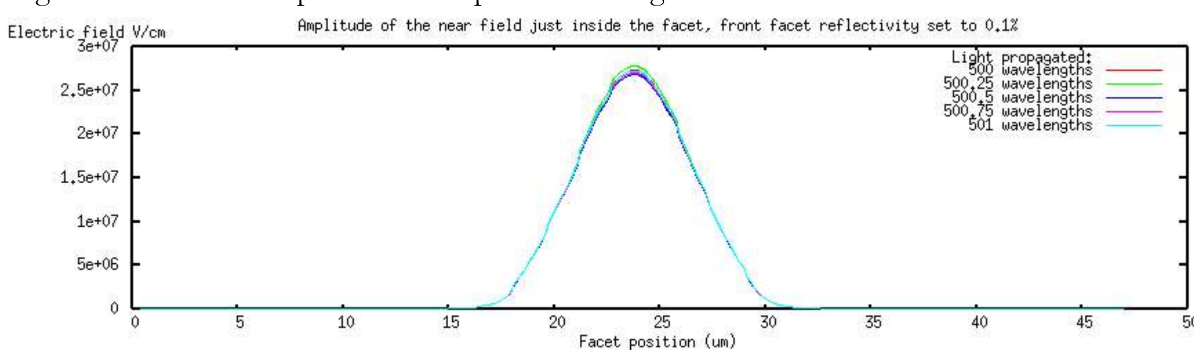

Figure 8.2a The amplitude of the near field in side the facet

The phase of the light accepted from the external optics and the light reflected off the internal mirror have once again, as in section 8.1 been plotted, in figures 8.2c,d respectively. It has been argued before (in section 8.1) that because the phase of the light reflected off the internal mirror decreases far more rapidly than the phase of the light being reflected off the external optics when the center of field reflected off the inside of front facet is perfectly in phase with the light being reflected off the external optics, constructive interference will occur. But however as one moves away from the central region field reflected off the front facet of the laser, the phase drops off very quickly which will mean the two fields will no longer be perfectly in phase thus the amount of constructive interference will decrease leading eventually to destructive interference. If one examines the sides of the main beam in figure 8.2a, it can be seen very clearly that very little constructive interference is occurring, one section out of of figure 8.2a has been expanded figure 8.2f. The most important thing about figure 8.2f is the amplitude of the green line compared to the amplitude of the blue line. At the beam's peak the green line representing a system in which the light was propagated through

500.25 meters produced the maximum constructive interference, and the blue line represented the system which produced maximum destructive interference. However at the beams edge , the situation is reversed for the reasons described above. This can be clearly be seen if one compares figure 8.2f and figure 8.2a, the the colors representing experiments have been kept the same in both graphs.

So far it has been demonstrated that back reflections from optics placed at about 250 wavelengths from the facet can play a major role in beam quality, in the next section the optics will be placed 500 wavelengths away from the facet.

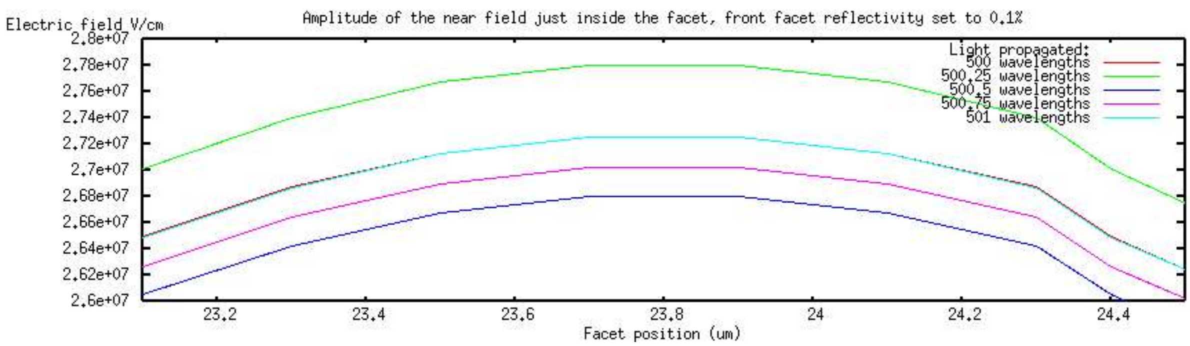

Figure 8.2b The amplitude of the near field in side the facet between 23.1 and 24.5um

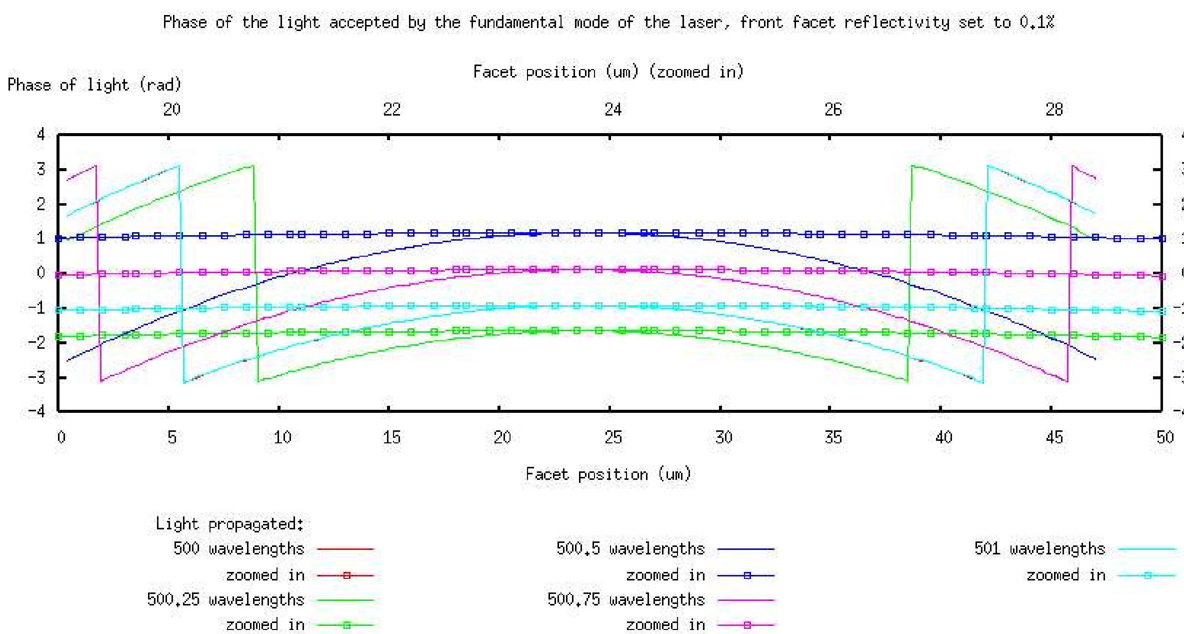

Figure 8.2c The phase of the light reflected back off the optics which has been accepted by the laser's fundamental mode.

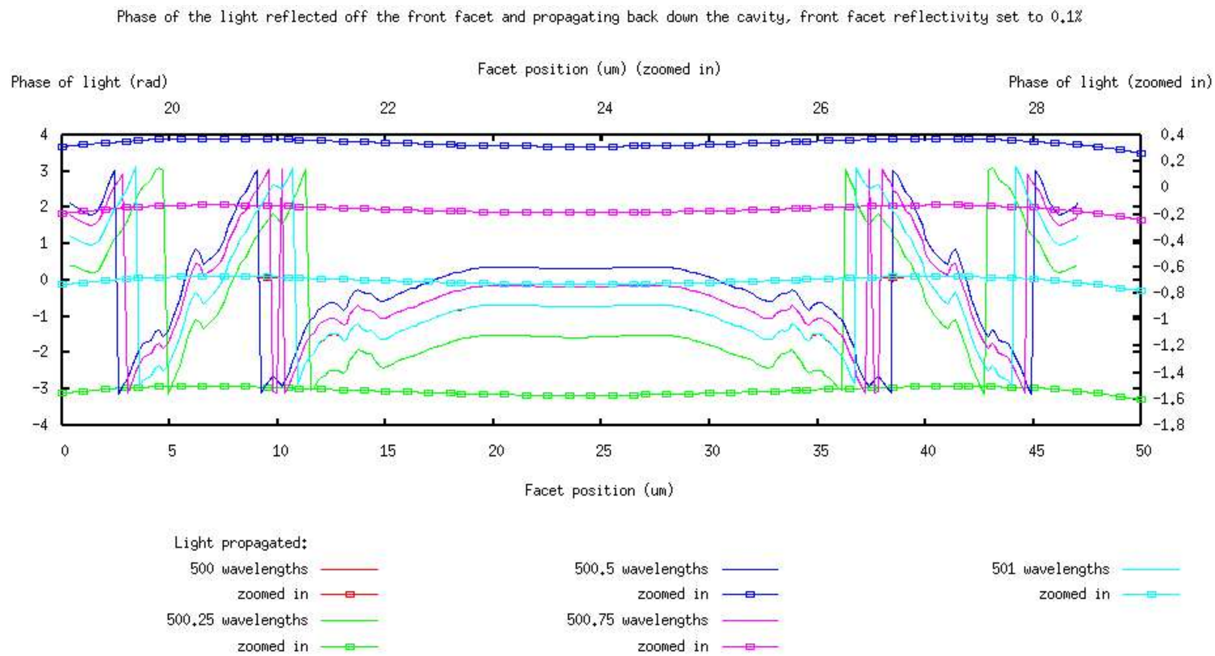

Figure 8.2d The phase of the light reflected off the front facet of the laser and now traveling back down the cavity.

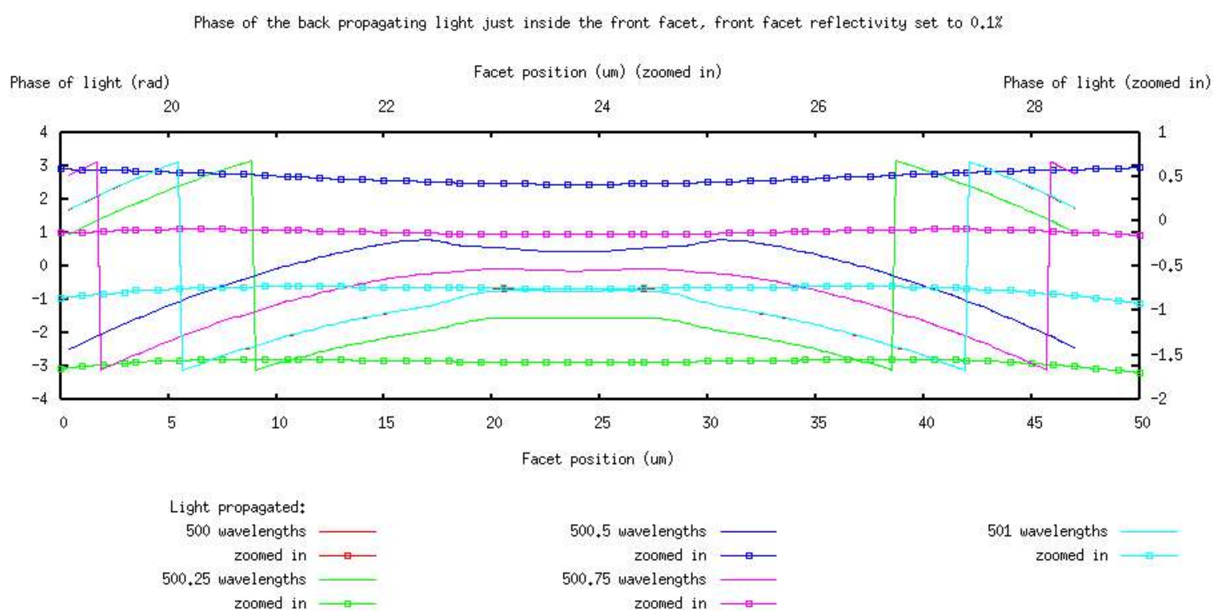

The phase of the combined field of the light accepted by the laser
and the light reflected off the internal mirror Figure 8.2e

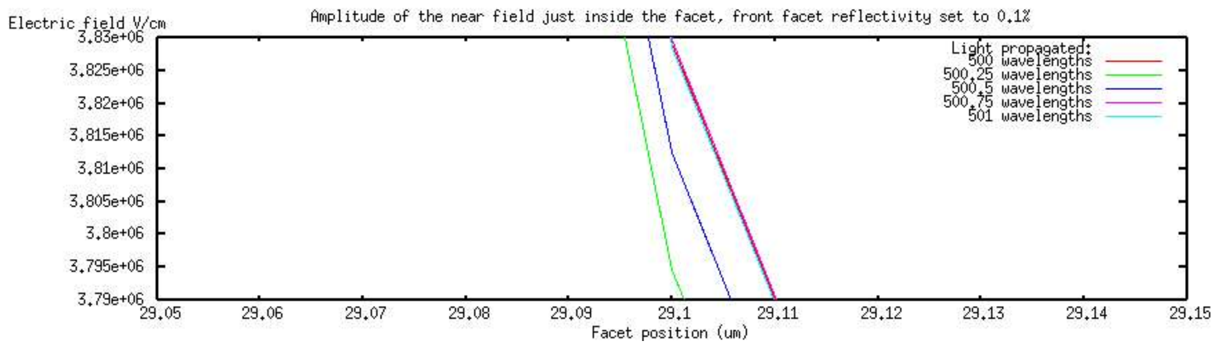

An expansion of figure 8.2a between 29.05 and 29.15um Figure 8.2f

The experiments performed in section 8.2 were repeated. This time the mirror was placed at about 500 wavelengths away from the laser, thus a total propagation distance of 1000-1001 meters was achieved. 500 wavelengths is a more reasonable distance for an optical component to be placed, it corresponds to about 0.5mm. The near field profile has been plotted in figure 8.3a,and an enlarged view of this has been plotted in figure 8.3b; on this graph for comparison has also been plotted the near field from experiments performed in section 8.2 when the total propagation distance was set to about 500 wavelengths. The first thing which is seen from this graph is that the fluctuation in amplitude of the mode due to to constructive and destructive interference is about the same even when the propagation distance has been doubled. Experiments were not performed for larger distances but this result suggests that back reflected light may affect the laser at much greater distances, however to establish this more experiments are required. The final observation that can be made from figure 8.3b is that generally all the tested systems which propagated their light through about 1000 wavelengths produce a near field with a lower amplitude than the systems which propagated their light through a distance of about 500 wavelengths.

This experiment has shown that doubling distance between the optics and the front facet does not decrease the level of fluctuation experienced when the length of the cavity is altered by values of less than one wavelength. This indicates that back reflections probably play an important role even if the optics were to be placed a considerable distance away. The reason for the decrease in mode height when the propagation distance is doubled is not clear. Guesses could be made, but that is all they would be.

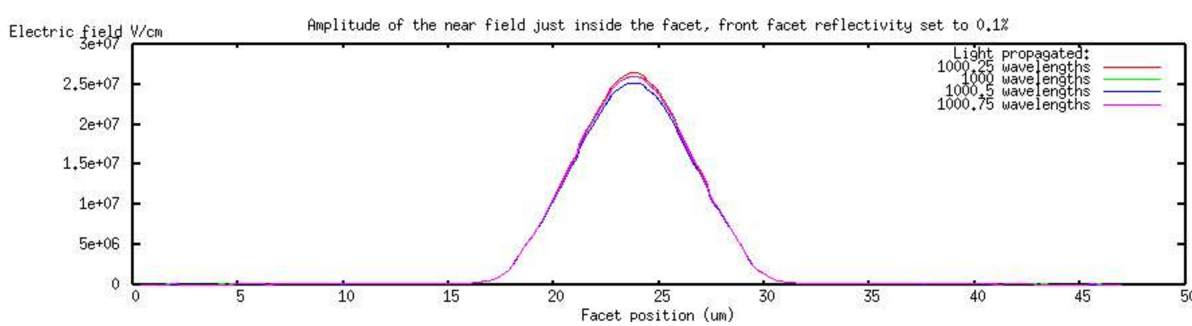

Figure 8.3a The amplitude of the near field in side the facet.

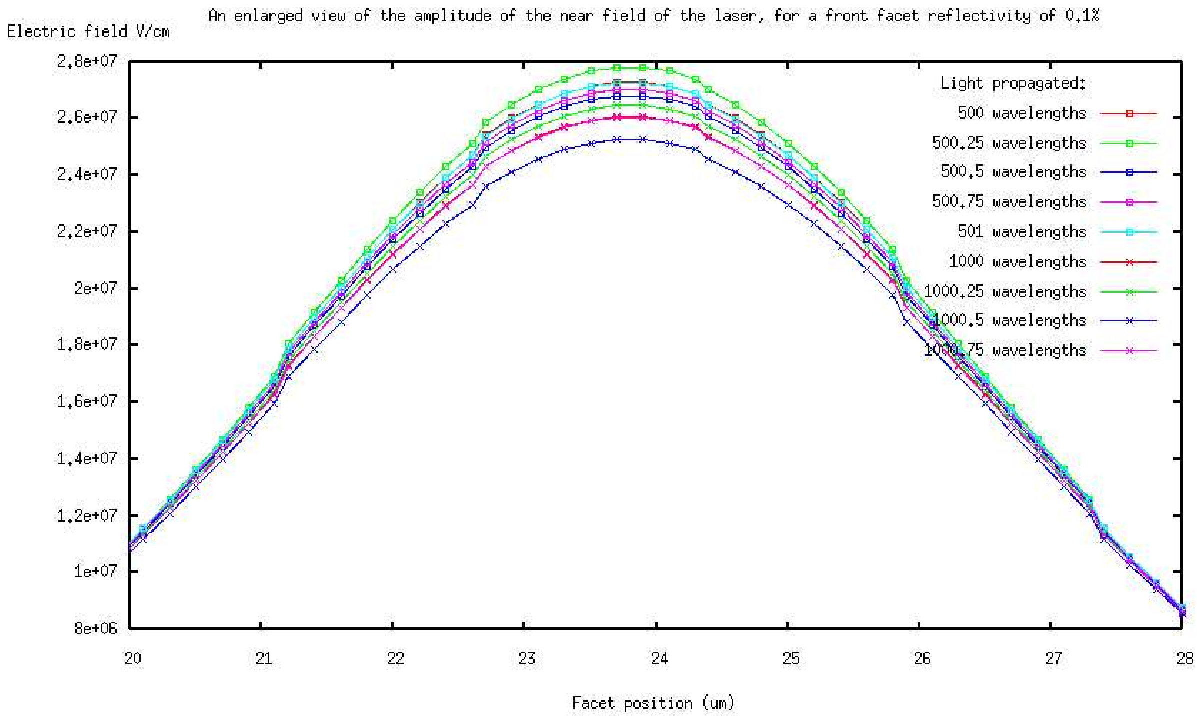

Figure 8.3b An enlarged view of the amplitude of the near field of the laser, for a front facet reflectivity of 0.1%.

9. Conclusion

The Overall conclusion

9.0 What has been learnt during the course of this project

Many things have been learnt during the course of this project. Each one will now be discussed in the following paragraphs.

- It has been demonstrated that feedback from optical components has a significant impact upon laser beam quality. Both the intensity of the beam and the horizontal mode shape have been shown to be significantly affected by feedback. It has been shown that the constructive and destructive interference between back-reflected light off the laser's front facet and the back reflected light off the optics coupled into the laser's fundamental mode is very important in this process.
- It has been shown that even if there is perfect constructive interference in the center of the beam between the the back reflected light from the optics and the back reflected light from the front facet. The light on the extremities of the back reflected beam returning to the master oscillator within the laser will no longer be perfectly in phase and may even destructively interfere. This is because of the slow drop off in phase of the back reflected light from the optics and the fast drop off in phase from the back reflected beam from the front facet. This effect improves beam quality by increasing the intensity of the light in the center of the beam and reducing it at the beam's extremities, thus narrowing of the beams width is observed. The reason for the back reflected light from the optics having a very slow change of phase at the facet compared to the light reflected off the front facet is that the back reflected light has *diffracted* out and thus the beam has spatially expand. This results in a much slower change of phase with distance. When this diffracted out beam reaches the facet again, it adds to the original beam shape which has not diffracted out. Thus, the facet is illuminated with light of almost constant phase which adds to the back reflected light reflected off the front facet whose phase varies rapidly with distance across the facet. The result is the above described constructive interference in the middle of the beam and destructive interference at the sides of the beam when the optical system is of an optimized nature. However if the system is un-optimized the mode quality can be degraded, as the center of the back reflected optical fields may be perfectly out of phase and as the phase changes across the laser facet the two fields may become more in phase, thus the laser's mode will spread.
  - Either the structure of the external optics, or more preferably, the laser could be altered to maximize the improvement in the mode shape.
- Variation of external cavity length by distances of under one wavelengths have been shown to have a large impact on beam quality. This brings into question the use of the external cavity for beam stabilization, unless effects such thermal expansion and changes in the air's optical characteristics with temperature and pressure can be compensated for - which is not likely.
- It has been shown that if one is aiming to significantly reduce the effects of optical feedback increasing the reflectivity of the front facet of the laser has proven to be a very effective tool.
- It was shown that lasers with front facets with a very low reflectivity are very susceptible to the effects of external feedback, which raises questions about their usefulness in optical systems however it has been shown that if the reflectivity is too large then beam quality can be degraded by effects such as spatial hole burning. This suggests that there may be some optimum value where

reflectivity is low enough to minimize effects such as spatial hole burning and high enough to prevent any problems with feedback from the external optics.

- It has been demonstrated that the level of fluctuation of light intensity at the center of the beam due to optical feedback is about the same when the optics are placed 250 λ away or 500 λ away. This suggests that this level of fluctuation may remain the same (thus remains a problem) even when the optics are moved further away.
- For each experiment with a different reflection coefficient on the front facet, different external cavity lengths were found to produce constructive or destructive interference at the center of the laser's beam. Probably because the three cavities, (the taper,the master oscillator and the external cavity) are each independent dynamic systems and neither operates with a fixed phase. Thus the back reflections from one can change the phase another emits.

All the experiments were performed with a narrow taper. Even so, the effects of feedback were substantial and would be expected to be more pronounced a larger taper angle.

9.1 To what extent were the project objectives achieved?

The best way to analyze the success of a project is to return to the project planning document, examine each objective set and then analyze to what extent it was achieved. In the following, section each goal within the project specification will be examined and a break down given as to the extent it was achieved.

"Aims and Objectives
The work will produce a software interface in LabVIEW that will bidirectionally couple the existing laser simulation software (CONAN) and the chosen existing optical modeling software."

A fully working bidirectional interface was produced which was used to run more than 300hours of simulations. There was no existing optical modeling software available. This meant that some custom software had to be written and the LabVIEW interface coupled with that.

"Investigations into how coupling optics and back reflections affect the mode shape/ beam quality will be carried out."

Three sets of experiments were conducted which examined the mode shape and beam quality. The results are presented above.

"Software Familiarization

- Familiarization with CONAN , the required inputs and the available outputs
- Learn how to simulate optical systems
- Learn how to use the graphical programming language LabVIEW
- Review the work of K.L. Ooi on the interfacing of LabVIEW with Conan."

All these objectives were achieved during the course of the project and of course K.L. Ooi's software was updated.

"Development of the LabVIEW interface

- Develop a bidirectional a interface capable of creating and reading the data files required by both CONAN and the chosen optical modeling software

- Calculate the overlap integral of the light reflected back from the optics and coupled back into the waveguide of the device"

The interface was developed and tested. The overlap calculation was calculated for the vertical mode of the laser and the mathematics were included in the LabVIEW interface as a vi.

"
- Investigate the effects of reflections between the output facet of the laser diode and the coupling lenses"

Lenses were modeled as sheets of BK7 glass. This sufficed to simulate cylindrical lenses as most of the back reflected light comes off the flat back surface on which the incident light falls. However, optical components such as the vertical collimator, due to its curved shape, could not be modeled with this approximation. The thin lens approximation could be used to model back reflections off such curved optical components. The software was carefully designed to be able to incorporate such modifications at a later stage. If a prewritten optical package had been used then this would not have been an issue. However, as custom software was being used, every feature added meant meant extra time spent writing software. This objective should be considered accomplished, but there is as much work in modeling different types of lenses with different antireflective coating as one wishes to do.

"
- Investigate the effects of lenses and filtering on the beam quality from a simulated laser diode."

Lenses were modeled, as was their impact on beam quality. Filtering was also experimented with by altering the front facet reflection coefficient.

I conclude the project objectives have all been achieved. Other useful things have also come out of the project along the way, such as an optical simulator and and an updated copy of K.L. Ooi's software.

9.2 Careful planning

This project had many elements which had to be finished on time, many of which were dependent on each other. The experiments which were run required planning, so that the computers were being used as much as possible. Accomplishing everything within the given time required careful time management. This point was recognized from the start. This is why extra care was taken in planning stages to produce a realistic Gantt chart. It was constantly updated to account for set backs, so that time was never wasted and no critical path broken. Without such careful planning of time, this project would never have been finished on time.

10. Further Work

A project is like sailing a boat up a river, as one sails up the river, it starts splitting off in to tributaries. One has to decide in which direction to go. One tributary may look more interesting than another, but sometimes one may wish to go in two directions as they both seem promising. However, one never has enough time to explore as much as one may like, so the best one can do is to note down the points of interest so that they can be returned to later. During this project areas which were worthy of further investigation were made note of, and will now be briefly described below.

1. Repeat the experiments with a wider variety of front facet reflectivities
2. Repeat the experiments with a larger distance between the laser and the optics
3. Explore designs of laser and optics which would produce constructive interference in the center of the beam and destructive interference at the edges of the beam , to try to improve the horizontal mode shape of the beam in a deliberate way.
4. Repeat the experiments performed during this project but examine the vertical mode shape variations across the facet, a 3D BPM simulator would be required for this.
5. Examine the possibility of inserting an optical isolator between the laser and the optics, although it may absorb too much energy and may also become damaged at high powers.
6. Coat the lens with some type of AR coating preventing back reflections in the first place.
7. Repeat the experiments with a wider taper, which may produce more feed back
8. Repeat the experiments for the realistic situation of a lens which is offset at an angle to the laser, i.e. Slightly skewed.
9. Introduce time domain modeling within the laser cavity. This would, however, require a more advanced laser simulator.
10. It would be worthwhile to confirm some of the computational results with experimental observations.
11. To repeat the simulation with 3D BPM would be very interesting.
12. CONAN assumes one lasing frequency, but composite cavities do perform frequency stabilization. Therefore, it would be interesting to re-run the simulations with a model which did not assume the lasing frequency.
13. An index guided device was used. It would be good to repeat the experiments with a gain-guided device, I expect theses devices may be less susceptible to the effects of optical feedback as the light is not confined to such a degree within the taper.
14. The optical simulator was good for what it had to do, but it would be worth while developing a far better and more flexible simulator.
15. The LabVIEW interface worked well, but as soon as one starts to develop a good custom optical simulator it would be worth while removing the this interface and incorporating it into the custom optical simulator. It may even be worth rewriting the entire optical simulator/LabVIEW interface in Fortran so it can be added into a library associated with CONAN.
16. The variation of the length of the external cavity by a fraction of a wavelength had a profound effect on the beam quality and mode shape. Therefore, it is uncertain whether an external cavity in practice would be a very useful outside a lab, as thermal expansion and humidity may effect the optical distance between the lens and the laser. However, it would be very interesting to investigate the effects of optical feedback on a laser which had two internal cavities.
17. Tapered lasers are often used in bars containing 20 or more lasing elements. It would therefore be interesting to see if any other affects were observed when there was optical feedback from more than one optical source on to a device. In fact as the the optical simulator considers the input field as periodic, it would therefore not be necessary to change the simulation set up at all – as long as one was content with assuming an infinitely long laser bar.

These are only a few thoughts for further development of the experiments and the tools which were used. This field is vast and there is more work to be done than could be possibly done in just a final year project. This project has laid the ground work for further investigations.

Appendix A

The derivation of the Fraunhofer Diffraction Equation used in the first optical simulator [15,40,19]

In this derivation we follow the relatively simple arguments presented in [15] to obtain the same results Goodman obtains obtains in [19] with a far more complex method. This section was included to explain the operation of the first optical simulator, and where the one over R term that caused all the problems came from. Figure 4.1 shows plain light waves incident upon an object which extends for infinity in the horizontal and vertical access, it has a small slit in its center. The light which falls upon the surface of the object is totally absorbed. The light which does not fall on the screen is propagated through the slit to a screen distance r away. The question now arises what image does the light produce on a screen placed distance r away.

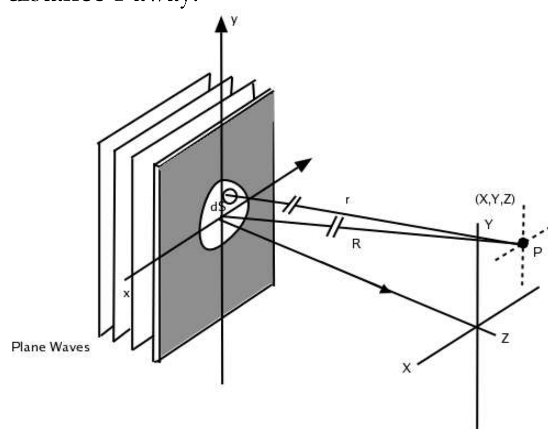

Plane waves incident on an object with an aperture cut in it Figure 4.1 adapted from [15]

The amplitude per unit area of the waves incident on the slit is defined as $E(x,y)(amplitude/m^2)$ We now consider an infinitely small area dS (which is essentially a point source which is often termed a Huygen wavelet[15]) Now the light emitted from this point source to point P has to be propagated to the screen at distance Z. By summing all the wavelets emanating from the slit and summing their amplitudes at point P we can calculate the amplitude of the light at point P.

The electric field generated by the wavelet must decrease in free space with a ratio of $\frac{1}{r}$ and there fore from fig 4.2 it would be reasonable to assume that

$$dE = \frac{E(x,y)dS}{r} e^{j(\omega t - kr)}$$

is valid. Where ω is the radial frequency, r is the distance propagated and k is the propagation constant in free space defined as $k=\frac{2\pi}{\lambda}$ where λ is the wavelength of the propagating light. The exponential takes account of the variance of the phase of the light with time and propagation distance.

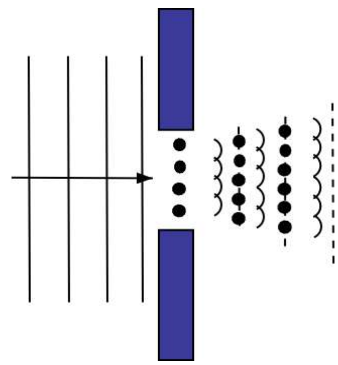

Figure 4.2 The concept of Huygens wavelets adapted from [15]

Which can be rewritten as

$$dE=\frac{E(x,y)dS}{r}\{e^{i\omega t}.e^{-ikr}\}\,dS$$

By Pythagorus the distance r can be calculated

$$R^2=X^2+Y^2+Z^2$$
$$r^2=(X-x)^2+(Y-y)^2+Z^2$$

$$solving\ for\ Z^2\ we\, can\, rewrite\, r^2$$
$$Z^2=R^2-X^2-Y^2$$
$$r^2=R^2-X^2-Y^2+(X-x)^2+(Y-y)^2$$
$$collecting\ the\ terms$$
$$r^2=R^2-Xx-2Yy+x^2+y^2$$

which can be written

$$r=R[1-\frac{2Xx+2Yy}{R^2}+\frac{x^2+y^2}{R^2}]^{\frac{1}{2}}$$

This can now be subsututed into the origonal result

$$dE=\frac{E(x,y)\cdot e^{i\omega t}\cdot e^{jkR[1-\frac{2Xx+2Yy}{R^2}+\frac{x^2+y^2}{R^2}]^{\frac{1}{2}}}}{R[1-\frac{2Xx+2Yy}{R^2}+\frac{x^2+y^2}{R^2}]^{\frac{1}{2}}}dxdy$$

which is the exact contribution of dE from the small point dxdy at point P.[15]

The approximation to the Fresnel diffraction integral[15,19]

If the slit is small and the distance of point P from the slit is relatively large then the denominator will be effectively constant across the whole screen thus it can be said that $R[1-\frac{2Xx+2Yy}{R^2}+\frac{x^2+y^2}{R^2}]\approx R$ where R is the distance of the screen. This simplifies the expression to

$$dE=\frac{E(x,y)\cdot e^{i\omega t}\cdot e^{jkR[1-\frac{2Xx+2Yy}{R^2}+\frac{x^2+y^2}{R^2}]^{\frac{1}{2}}}}{R}dxdy$$

however this approximation can not be made with the phase because of the short wavelength of the light, a small change in distance to the screen will affect the phase substantially.

So if the binomial expansion of $(1-x)^{\frac{1}{2}}=1-\frac{x}{2}-\frac{x^2}{8}....$ only keeping the first two terms, the expression can be written as .

$$dE=\frac{E(x,y)\cdot e^{i\omega t}\cdot e^{jk[R-\frac{Xx+Yy}{R}+\frac{x^2+y^2}{2}R]}}{R}dxdy$$

So far we have calculated the field at a point P on a screen due to a small patch dS of radiation from a slit. But what we want is the total combined radiation due to all the small patches dS at point P, this is calculated with the equations

$E(P)=\int dE$

Which results in

$$E(X,Y)=\iint\frac{E(x,y)\cdot e^{i\omega t}\cdot e^{jk[R-\frac{Xx+Yy}{R}+\frac{x^2+y^2}{2}R]}}{R}dxdy$$

The astute reader will have noticed that there is a dimensional miss match as E(X,Y) has units $amplitude/meter$ and should have $amplitude/meters^2$ many authors introduce a 'constant' in the derivation in order to take account of this, for our purposes it will be taken that this constant is included in the $E(x,y)$ term. Goodman [19] using a different approach which spans first section to his book and is to long to be included here derives the equation in a slightly different way and gets a few extra constants resulting in the following equation.

$$E(X,Y)=\frac{e^{jkR}}{j\lambda R}e^{j\frac{k}{2R}(X^2+Y^2)}\iint_{-\infty}^{\infty}\{E(X,Y)e^{\frac{-jk}{2R}(x^2+y^2)}e^{-j\frac{2\pi}{\lambda R}(Xx+Yy)}\}dx\,dy$$

This is called the Fresnel diffraction integral. And is in fact is in the form implemented in the first optical simulation software. This was implemented in a discrete form for implementation in software.

$$E(X,Y)=\frac{e^{jkR}}{j\lambda R}e^{j\frac{k}{2R}(X^2+Y^2)}\sum_{x=-\infty}^{\infty}\sum_{y=-\infty}^{\infty}\{E(x,y)e^{\frac{-jk}{2R}(x^2+y^2)}e^{-j\frac{2\pi}{\lambda R}(Xx+Yy)}\}$$

Reference

[1] L. Borruel,S. Sujecki M. Krakowski,B. Sumpf, P.Moreno,J. Wykes,S.C Auzanneau, G. Erbert, D. Rodriguez, P.Sewll,M. Calligaro, H. Wenzel, T.M. Benson, E.C. Larkins and I. Esquivias. High Brightness Tapered Lasers at 735nm and 975nm experiments and numerical analysis

[2] S. Sujecki, L. Borruel, . Wykes, P.Moreno, B.Sumpf, P. Sewell, H.Wenzel, T.M. Benson, G. Erbert, I. Esquivias, E.C. Larkins Non-linear properties of tapered laser cavities.

[3] Fukuda, Mitsuo A pratical guide to industrial applications of optical semiconductor devices

[4] B. Streetman Solid State Electronic Devices

[5] H.-G. Unger, "Elektromagnetische Wellen auf Leitungen 4. Auflage" 1996

[6] N. Chinone, K. Aiki and R. Ito "Stabilization of semiconductior laser outputs by a mirror close to a laser facet" Appl. Phys. Lett. 15 December 1978

[7] Roy Lang and Kohroh Kobayashi "External Optical feedback Effects on Semiconductor Injection Laser Properties" IEEE Journal of quantum electronics, VOL, QE-16, NO. 3 March 1980 P347

[8] A.P Bogatov, P.G. Eliseev, L.P. Ivanov, A.S. Logginov, M.A. Manko and K. YA Senatorov "Study of the Single-Mode Injection Laser", IEEE Journal of Quantum Electroics 1973, P392

[9] N. Chinone, K. Aiki and R. Ito "Stabilization of semiconductor laser outputs by a mirror close to a laser facet" Appl. Phys. Lett., Vol.33 No. 12 15 December 1978 P993

[10] G. Erbert, J. Fricke, R. Huelsewede, A. Knauer, W. Pittoff, P. Ressel, J. Sebastiam, B. Sumpf, H. Wenzel and G. Traenkel 3W – high brightness tapered diode lseres at 735nm based on tensile strained GaAsP-QWs

[11] E.S. Kintzer, .N. Walpole, S.R. Chinn, C.A. Wang and L.J. Missagia "High-Power, Strained-Layer Amplifiers and Lasers with Tapered Gain Regions" IEEE Photinics Technology Letters Vol 5, NO 6 P605

[12] Sylvie Delepine, Frank Gerard, A. Pinquier, T. Fillon, . Pasquier, D. Locatelli, .P. Chardon, Hans K. Bissesur, . Bouche, Francois R. Bouabl, and Paul Saler "How to Launch 1W Into Single-Mode Fuber From a Single 1.48um Flared Resonator" IEEE ournal on Selected topics in quantum electronics Vol. 7 March/April 2001 P 111

[13] D.J. Bossert, J.R. Marciante, and M. W. Wright, "Feedback effects in tapered broad-area semiconductio lasers and amplifyers" IEEE Photon Technol Lett, vol. 17 pp 470-472, May 1995

[14] Dr. S. Sujecki Mr. J Wykes Dr. P Sewell Professor T M Benson Professor E C Larkins The School of Electrical and Electronic Engineering. Manual for the Integrated Laser Diode Simulation Package (ILDSP) The Control Module and The Optical Module March 2003

[15] Raymond G. Wilson "Fourier Series and Optical Transform Techniques in Contemporay Optics." Wiley-interscience 1995 Chapter 5

[16] Dr. G.H. Cross E-Mode Propagation, Local Normal Modes and Waveguide Transitions. www.dur.ac.uk/gh.cross/notes_.pdf Accessed on 1st February 2004.

[17] http://aanda.u-strasbg.fr:2002/articles/astro/full/2000/14/ds9289/node2.htm

[18] J.A. Ratcliffe. Aspects of diffractioon theory and their application to the ionosphere. In AC Strickland, editor, Reports on Progress in Physics, volume XIX. The Physical Society, Lonfon, 1956

[19] Introduction to Fourier Optics Joseph W. Goodman, Second Edition, McGrawHill, 1986
[20] Fields and waves in communication electronics Simon Ramo John R. Whinnery Theodore Van Duzer. Third Edition Wiley ISB 0-471-58551-3
[21]M. Mikulla, P. Chazan, A. Schmitt, S. Morgott, A. Wetzel, M. Walther, R. Kiefer,
High-Brightness Tapered Semiconductor Laser Oscillators and Amplifiers with Low-Modal Gain Epilayer-Structures W. Pletschen, J. Braunstein, and G. Weimann, Member, IEEE PHOTONICS TECHNOLOGY LETTERS, VOL. 10, NO. 5, MAY 1998
[22] Fundamentals of Photonics, Saleh,Teich, Wiley Interscience. 1991
[23] A. Al-Muhanna, L. J. Mawst, D. Botez, D. Z. Garbuzov, R. U. Martinelli, and J. C. Connolly, "14.3 W quasicontinuous wave front-facet
power from broad-waveguide Al-free 970 nm diode lasers," *Appl. Phys. Lett.,* vol. 71, pp. 1142–1145, 1997.
[24] G.P. Agrawal, Fiber-Optic Communication Systems, Wiley, New York, 1997.
[25] P. Günter (Ed.), Nonlinear Optical Effects and Materials, Series in Optical Sciences, Vol. 72, Springer, Berlin, 2000.
[26] IEEE J. Select. Topics Quantum Electron. 6 (2001), Special Issue on Lasers in Medicine and Biology.
[27] W. Schulz, R. Poprawe, Manufacturing with novel high-power diode lasers, IEEE J. Select. Topics Quantum Electron. 6 (2000) 696–705.
[28] http://www.wsi.tu-muenchen.de/E26/en/research/longwave/structures.html "A picture of a ridge wave guide"
[29] Intergrated optics edited by T. Tarmir with cintributions by E. Garmire [et al.]
[30] Intergrated optics : design and modeling /Reinhard März
[31] J. Marciu J. L. Auguste and J.M. Blondy "Cylindrical 2D Beam Propagation Method for Optical Structires Maintaining a Revolution System" Optical fibre Technology 5 105-118 (1999) accessed via www.sciencesdirect.com
[32] E-G. Neumann Single Mode Fibers Fundamentals Springer Series in Optical Sciences 1998 pp172
[33] Goubau G.: On the excitation of surface waves. Proc. IRE, 40, 1952 865-868
[34] Jones A.L. Coupling of optical fibers and scattering in fibers. . Opt. Soc. Am. 55, 261-271 1965
[35] Marcuse 1970b Bell. Syst. 40 273-298
[36] Kapany et. al. September 1970 J. Op. Soc. Am. Vol.60 Number 9 pp1178-1185
[37] A.W Snyder May 1966 pp606 J. Op. Soc. Am, Vol 56 Num. 5
[38]Madrid Manual for the Electrical and Thermal Part of the Integrated Laser Diode Simulation Package (ILDSP) I. Esquivias, L. Bottuel, Departamento de Tecnologia Fotonica ETSI Telecomunication Universidad Politecnica de
[39]HAROLD version 3.0 ser Manual Departamento de Tecnologia Fotonica ETSI Telecomunication Universidad Politecnica de Madrid Manual
[40] J. Gaskill, Linear Systems, Fourier Transforms and Optics Wiley and Sons Inc.
[41]High-Speed Optielectronic VLSI Switching Chip with >4000 I/O Based on Flip-Chip Bonding of MQW Modulators and Detectors to Silicon CMOS April 1996 pp77 Anthony L. Lentine et. al.
[42] 3-D Intergration of MQW Modulators over Active Submicron CMOS Circuit: 375 Mb/s Transimpedance Receiver-Transmitter Circuit D.A.B Miller et. Al IEEE Photonics Technology Letters Vol 7 No 1 November 1995
[43]GaAs MQW Modulators Integrated with Silicon CMOS K.W. Goosen J.A. Walker L.A. D'Asaro et. al. IEEE Photonics Technology Letters Vol.7 No 4. April 1995
[44] Dr. Matthew Clark's Thesis http://optics.eee.nott.ac.uk/optics/downloads/direct_search.

Index